JOURNAL OF GEOPHYSICAL RESEARCH, VOL. 105, NO. D19, PAGES 24,283–24,304, OCTOBER 16, 2000

Quantitative constraints on the atmospheric chemistry of nitrogen oxides: An analysis along chemical coordinates

R. C. Cohen,[1,2] K. K. Perkins,[3] L. C. Koch,[1,4] R. M. Stimpfle,[5] P. O. Wennberg,[6] T. F. Hanisco,[5] E. J. Lanzendorf,[5] G. P. Bonne,[5,7] P. B. Voss,[5] R. J. Salawitch,[8] L. A. Del Negro,[9,10] J. C. Wilson,[11] C. T. McElroy,[12] and T. P. Bui[13]

Abstract. In situ observations of NO_2, NO, NO_y, $ClONO_2$, OH, O_3, aerosol surface area, spectrally resolved solar radiation, pressure and temperature obtained from the ER-2 aircraft during the Photochemistry of Ozone Loss in the Arctic Region in Summer (POLARIS) experiments are used to examine the factors controlling the fast photochemistry connecting NO and NO_2 and the slower chemistry connecting NO_x and HNO_3. Our analysis uses "chemical coordinates" to examine gradients of the difference between a model and precisely calibrated measurements to provide a quantitative assessment of the accuracy of current photochemical models. The NO/NO_2 analysis suggests that reducing the activation energy for the $NO+O_3$ reaction by 1.7 kJ/mol will improve model representation of the temperature dependence of the NO/NO_2 ratio in the range 215-235 K. The NO_x/HNO_3 analysis shows that systematic errors in the relative rate coefficients used to describe NO_x loss by the reaction OH + $NO_2 \rightarrow HNO_3$ and by the reaction set $NO_2+O_3 \rightarrow NO_3$; $NO_2+NO_3 \rightarrow N_2O_5$; $N_2O_5+H_2O \rightarrow 2HNO_3$ are in error by +8.4% (+30/-45%) (OH + NO_2 too fast) in models using the Jet Propulsion Laboratory 1997 recommendations [DeMore et al., 1997]. Models that use recommendations for $OH+NO_2$ and $OH+HNO_3$ based on reanalysis of recent and past laboratory measurements are in error by 1.2% (+30/-45%) (OH + NO_2 too slow). The +30%/-45% error limit reflects systematic uncertainties, while the statistical uncertainty is 0.65%. This analysis also shows that the POLARIS observations only modestly constrain the relative rates of the major NO_x production reactions $HNO_3 + OH \rightarrow H_2O + NO_3$ and $HNO_3 + h\nu \rightarrow OH + NO_2$. Even under the assumption that all other aspects of the model are perfect, the POLARIS observations only constrain the rate coefficient for $OH+HNO_3$ to a range of 65% around the currently recommended value.

1. Introduction

Odd-nitrogen radicals, NO_x ($NO_x \equiv NO + NO_2$), affect the rate of chemical removal of ozone in the stratosphere by direct catalysis [*Crutzen*, 1971; *Johnston*, 1971] and by their indirect influence over the abundance of hydrogen and halogen radicals [e.g., *Wennberg et al.*, 1994b]. Experiments designed to observe the distribution of stratospheric NO_x and to use atmospheric observations to test models of stratospheric NO_x chemistry have a long history [e.g. *Noxon*, 1975]. Recent efforts include multiyear observations of the column abundance of NO_2 and HNO_3 from the surface [*Koike et al.*, 1994; *Solomon et al.*, 1994; *Slusser et al.*, 1998], remote sensing observations of NO, NO_2, HNO_3, $ClONO_2$, and N_2O_5 from balloons and space [*Roche et al.*, 1994; *Gordley et al.*, 1996; *Newchurch et al.*, 1996; *Kumer et al.*, 1997; *Mickley et al.*, 1997; *Zhou et al.*, 1997; *Sen et al.*, 1998; *Osterman et al.*, 1999], and high spatial resolution in situ measurements of NO_y or its major components from balloons and aircraft ($NO_y \equiv HNO_3 + 2 \times N_2O_5 + ClONO_2 + BrONO_2 + NO_2 + NO + HO_2NO_2 + NO_3 + \ldots$) [*Webster et al.*, 1994a; *Weinheimer et al.*, 1994; *Gao et al.*, 1997, 1999]. Analysis of these (and numerous other) observations have improved our understanding of $NO_x \Leftrightarrow NO_y$ photochemistry. The recognition that N_2O_5 is hydrolyzed on about 1 in 10 collisions with a sulfate aerosol was a crucial step in developing a more accurate model [e.g., *Mozurkewich and Calvert*, 1988; *McElroy et al.*, 1992; *Fahey et al.*, 1993]. Inclusion of this reaction in models of stratospheric nitrogen oxides is essential to simultaneously describing the wealth of observations taken before, during, and after the Mount Pinatubo eruption and confirms speculation that this reaction is important to stratospheric chemistry that dates back at least to *Johnston* [1971] and to the detailed analysis of *Cadle et al.* [1975].

[1]Department of Chemistry, University of California, Berkeley.
[2]Department of Earth and Planetary Science, University of California Berkeley. and Energy and Environment Division, Lawrence Berkeley National Laboratory, Berkeley, California.
[3]Department of Earth and Planetary Sciences, Harvard University, Cambridge, Massachusetts.
[4]Now at Department of Chemistry, University of Colorado, Boulder.
[5]Department of Chemistry and Chemical Biology, Harvard University, Cambridge, Massachusetts.
[6]Divisions of Engineering and of Geological and Planetary Sciences, California Institute of Technology, Pasadena.
[7]Now at Electric Power Research Institute, Palo Alto, California.
[8]Jet Propulsion Laboratory, California Institute of Technology, Pasadena.
[9]Aeronomy Laboratory, NOAA, Boulder, Colorado.
[10]Now at Climate Monitoring and Diagnostics Laboratory, NOAA, Boulder, Colorado.
[11]Department of Mechanical Engineering, University of Denver, Denver, Colorado.
[12]Environment Canada, Downsview, Ontario.
[13]Ames Research Center, NASA, Moffett Field, California.

Paper number 2000JD900290.
0148-0227/00/2000JD900290$09.00

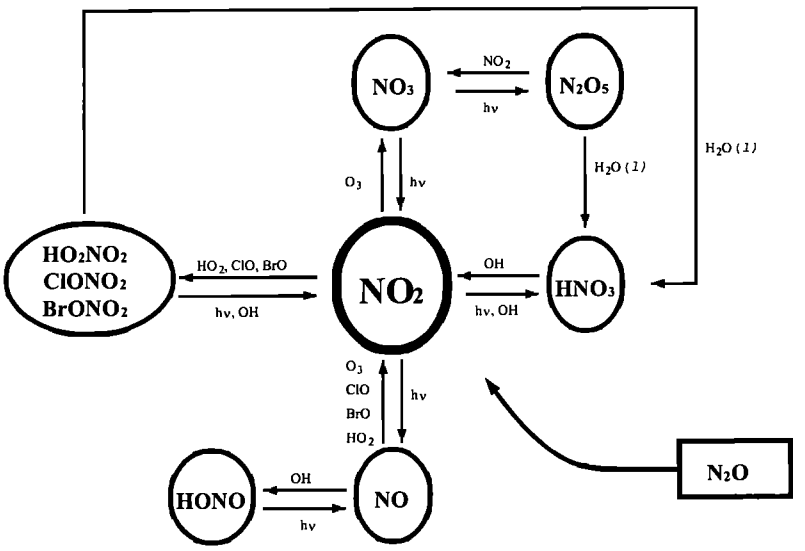

Figure 1. Stratospheric NO_x and NO_y photochemistry

Quantitative evaluation of the accuracy of $NO_x \Leftrightarrow NO_y$ photochemistry by comparison of photochemical models to stratospheric measurements remains a significant challenge: the large number of competing reactions involved (Figure 1 and Table 1) make it difficult to isolate the effects of individual reactions; the long photochemical lifetime of $[NO_x]$ (~2-30 days) makes it difficult to unambiguously separate the effects of chemistry from those of transport; and the technology does not yet exist to make accurate, precise, and simultaneous measurements of all of the trace species involved on spatial scales small compared to chemical gradients within the atmosphere (e.g. in situ N_2O_5, $BrONO_2$, HO_2NO_2) nor to make remote observations of free radicals (especially OH and HO_2) with the accuracy and precision necessary to quantitatively constrain our understanding. Another limitation is that no direct, straightforward procedure for comparing the chemical information (as distinct from the geophysical information) contained in measurements made in different locations, at different times, or by different suites of instruments has been articulated.

Measurements obtained using the ER-2 platform during the Photochemistry of Ozone Loss in the Arctic Region In Summer (POLARIS) experiments in 1997 and laboratory measurements of the rate coefficients for the reaction $OH+NO_2$ by *Donahue et al.* [1997], *Dransfield et al.* [1999] and for the reactions $OH+NO_2$ and $OH+HNO_3$ by *Brown et al.* [1999a, 1999b] have inspired renewed examination of our knowledge of $NO_x \Leftrightarrow NO_y$ photochemistry. Analyses of POLARIS observations by *Gao et al.* [1999] and *Osterman et al.* [1999] conclude that the new laboratory rate coefficients improve the ability of photochemical models to reproduce observations of the NO_x/NO_y ratio. *Drdla et al.* [1999] examine a suite of heterogeneous reactions, including $H_2CO + HNO_3$ and $HONO+HNO_3$, to show that solutions to the model-measurement discrepancy proposed by *Gao et al.*, [1999] and *Osterman et al.* [1999] are not unique and that photochemical mechanisms that are not represented in current models could, within the bounds of reasonable uncertainties, have a measurable impact on models of NO_x to NO_y ratios. *Wennberg et al.* [1999] use high solar zenith angle HO_x observations from POLARIS to suggest that HNO_4 might be a

Table 1. Reactions Involved in the Photochemical Control Over NO_x in the Lower Stratosphere.[a]

Reaction Number	Reaction
	NO_x Production
(R1)	$HNO_3 + OH \rightarrow NO_3 + H_2O$
(R2)	$HNO_3 + h\nu \rightarrow NO_2 + OH$
(R3)	$N_2O_5 + h\nu \rightarrow NO_2 + NO_3$
(R4)	$ClONO_2 + h\nu \rightarrow NO_2 + ClO; NO_3 + Cl$
(R5)	$BrONO_2 + h\nu \rightarrow NO_2 + BrO; NO_3 + Br$
(R6)	$HO_2NO_2 + h\nu \rightarrow NO_3 + OH; NO_2 + HO_2$
(R7)	$HO_2NO_2 + OH \rightarrow$ products
	NO_x Loss
(R8)	$NO_2 + OH \xrightarrow{M} HNO_3$
(R9)	$NO_2 + ClO \xrightarrow{M} ClONO_2$
(R10)	$NO_2 + BrO \xrightarrow{M} BrONO_2$
(R11)	$NO_2 + NO_3 \xrightarrow{M} N_2O_5$
(R12)	$NO_2 + HO_2 \xrightarrow{M} HO_2NO_2$
	NO_y Cycling
(R13)	$N_2O_5 +$ aerosol $\rightarrow 2\ HNO_3$
(R14)	$ClONO_2 +$ aerosol $\rightarrow HOCl + HNO_3$
(R15)	$BrONO_2 +$ aerosol $\rightarrow HOBr + HNO_3$
	NO_x Cycling
(R16)	$NO + O_3 \rightarrow NO_2 + O_2$
(R17)	$NO + ClO \rightarrow NO_2 + Cl$
(R18)	$NO + BrO \rightarrow NO_2 + Br$
(R19)	$NO + HO_2 \rightarrow NO_2 + OH$
(R20)	$NO_2 + h\nu \rightarrow NO + O$
(R21)	$NO_2 + O_3 \rightarrow NO_3 + O_2$
(R22)	$NO_3 + h\nu \rightarrow NO_2 + O$

[a] Reactions involving N atoms, and HONO have been neglected.

smaller component of NO_y than current photochemical models predict.

In this paper, we evaluate elements of photochemical models describing nitrogen radical abundance using an approach based on "chemical coordinates" that allows quantitative and systematic discussion of the comparison between models and measurements. Through most of the analysis, we assume that current photochemical models are complete. We use the analysis along chemical coordinates to constrain the range of reaction rate coefficients that are consistent with observations of atmospheric composition and where possible to place bounds on uncertainties in rate coefficients that are smaller than those estimated on the basis of laboratory observations alone. We also place some limits on the maximum impact of "missing chemistry" (processes not represented by the model), subject to the assumption that the existing models and observations are perfectly accurate.

The chemical coordinates are defined as the parameters that appear directly in the photochemical equations describing the abundance or ratio of abundances of the chemical species of interest. For example, a series of experiments beginning at sunset and observing both the decay of NO_2 and the increase in HNO_3 would have chemical coordinates that could be used to constrain the uncertainty in the rates of the three reactions below directly from observations [e.g. *Webster et al.*, 1990]:

(R21) $NO_2+O_3 \rightarrow NO_3+O_2$

(R11) $NO_2+NO_3 \xrightarrow{M} N_2O_5$

(R13) $N_2O_5+H_2O \xrightarrow{\text{Aerosol}} 2\ HNO_3$.

Chemical coordinates for the R11-R13-R21 reaction system include temperature, ozone, pressure, aerosol, H_2O, NO_2, NO_3, N_2O_5, HNO_3, and time. For warm stratospheric temperatures it might be necessary to expand the reaction set to include N_2O_5 thermal decomposition. Geophysical variables including latitude or altitude are not chemical coordinates; tracers such as N_2O or CFC-11 are not chemical coordinates, although in a practical experiment it may be essential to have tracer measurements to demonstrate that observations obtained at different times were made in the same air mass.

Analysis of observations using chemical coordinates simplifies interpretation of the quantitative constraints on rate coefficients that can be derived from the average agreement between models and a suite of observations. There are some obvious points worth emphasizing. First, each point in the phase-space of the chemical coordinates is unique. Measurements at any given point in phase-space should be identical (within experimental uncertainty), regardless of when or where in the atmosphere they are obtained or whether they are obtained with the same experimental payload. This property of the chemical coordinates can be used to evaluate whether a new measurement provides a constraint on a poorly sampled aspect of the atmospheric chemistry or adds to the statistical weight of prior observations. Second, observations that span a wide range in these coordinates contain more chemical information than observations obtained at a single point. Third, as we discuss in detail below, the gradient of the agreement with respect to the chemical coordinates can be used to focus attention on the accuracy of particular subsets of chemical reactions within a model. In favorable cases, such gradients can be used to explicitly isolate the derivatives of the model with respect to each of the individual chemical coordinates while holding the position in all other coordinates constant. In this way, one can test the accuracy of the model derivatives directly against atmospheric observations. Finally, the chemical coordinates organize observations along lines represented by the mechanisms that control chemical abundances. In the chemical coordinate framework, we expect a smooth continuous function connecting those measurements that exhibit "good agreement" with the "exceptions." This organization along chemical coordinates helps to shift attention from differences that might be associated with geophysical variables (e.g. latitude, season, year) or experimental variables (flight number) to the variables that are coupled more directly to the photochemistry of the atmosphere.

The approach to quantifying our understanding of NO_x/NO_y photochemistry developed in this paper is a natural extension of methods we used to place quantitative constraints on the fast photochemistry connecting OH to HO_2 [*Cohen et al.*, 1994], and ClO to $ClONO_2$ [*Stimpfle et al.*, 1994, 1999] and to examine photochemistry of OH [*Salawitch et al.*, 1994; *Wennberg et al.*, 1999]. In those papers, we evaluated the accuracy of model descriptions of the derivatives $\partial[HO_2]/\partial[NO]$, $\partial[HO_2]/\partial[O_3]$, $\partial[ClO]/\partial[NO_2]$, and $\partial[OH]/\partial$(solar zenith angle) demonstrating that models of OH/HO_2 and $ClO/ClONO_2$ reproduce the dependence on NO_x more accurately than expected given the uncertainties in laboratory rate coefficients and that OH radicals have one or more sources that are not (or were not at the time of publication) represented by the current models. Each of these papers attempted to isolate the variable of interest while holding all other relevant factors constant. Studies by *Fahey et al.* [1993], *Dessler et al.* [1996], and *Jaegle et al.* [1994] have taken a similar approach to analysis of $\partial[NO_x/NO_y]/\partial$[aerosol surface area], $\partial[ClO]/\partial[ClONO_2]$, and $\partial[NO]/\partial[O_3]$, respectively. *Jucks et al.* [1999] use the chemical coordinates defined in section 4 of this paper to discuss comparison of their observations of HNO_3 and NO_2 to models.

The POLARIS experiments represent a unique opportunity to use a chemical coordinate approach to understanding NO_x and NO_y photochemistry:

1. An informal intercomparison of measurements of NO_2, using two fundamentally different experimental approaches, substantially increases our confidence that this species is being measured accurately. Accurate NO_2 measurements are central to this analysis, since nearly every important NO_x loss process involves NO_2 (Figure 1).

2. Simultaneous observations of OH, and a thorough knowledge (if not a complete understanding) of the diurnal variation of lower stratospheric OH [*Wennberg et al.*, 1994b, 1999], reduce what would otherwise be a significant uncertainty in the analysis. Hydroxyl concentrations are particularly important to any empirical test of NO_x/NO_y photochemistry. For example, we calculate that reactions of OH are responsible for between 40% and 60% of the NO_x production ($OH + HNO_3 \rightarrow H_2O + NO_3$, R_4) and for 20% to 98% of NO_x loss ($OH + NO_2 \rightarrow HNO_3$, R_{11}) in the air sampled by the ER-2 during POLARIS. The OH concentrations used in our analysis are constrained to be in agreement with observations. Many previous analyses of NO_x/NO_y simultaneously model both OH and NO_x concentrations. Because of the strong coupling between OH, NO_2 and HNO_3 concentrations, analyses that use modeled OH concentrations can mask discrepancies between model and observation through compensating errors.

3. The first in situ observations of $ClONO_2$ [*Stimpfle et al.*,

1999; *Bonne et al.*, 2000] show that current models of the $ClO/ClONO_2$ are accurate. These measurements strongly suggest that errors (if any) in the interpretation of laboratory measurements of pressure dependence of photolysis quantum yield for $ClONO_2$ (and hence in models of the $ClO/ClONO_2$ ratio in the lower stratosphere) which *Nickolaisen et al.* [1996] suggested might be large are small. If there had been a large error then the atmosphere would have contained higher than expected $ClONO_2$ concentrations and consequently lower than expected HNO_3 fractions of NO_y.

4. Finally, we have an improved understanding of how to treat the solar radiation field. Analysis of POLARIS observations of OH, NO, NO_2 and NO_y by *Perkins* [2000] shows that the photolysis rates are demonstrably more precise when they are computed using the overhead ozone derived from onboard, spectrally resolved measurements of the radiation field using the Composition and Photodissociative Flux Measurement (CPFM) than when they are inferred from scaling a climatological vertical profile for O_3 to the total column measured by the Total Ozone Mapping Spectrometer (TOMS). Analyses by both *Perkins* [2000] and P.B. *Voss, et al.* (Chlorine Partitioning in the lower stratosphere: A comparison of modeled and measured $ClONO_2/HCl$ during POLARIS, submitted to J. Geophys. Res, 2000) show that using the average albedo experienced by an air parcel along its back trajectory or zonally averaged albedo leads to a more precise representation of photochemical systems with time constants of more than 1 day than if one employs the instantaneous albedo at the time of the observation. The lack of a diagnostic for the precision of the radiation field has hampered prior attempts to ascertain the cause of model-measurement discrepancies, as has the difficulty of accurately accounting for the effects of air parcel history.

2. Observations, Photolysis Rates, and Photochemical Calculations

The POLARIS experiments include 25 flights of the ER-2 aircraft between April and September 1997. The majority of these flights originated from Fairbanks, Alaska (65°N, 150°W). Flights also originated at NASA Ames (37°N, 122°W) and Barbers Point, Hawaii (21°N, 150°W) extending the latitudinal range from the pole to the equator.

2.1. NO_2 Observations

The POLARIS campaign marked the debut of an instrument designed for the in situ detection of an array of halogen and nitrogen radicals and their precursors from the NASA ER-2 aircraft. The instrument expands the capabilities of its precursor, designed to detect ClO and BrO [*Brune et al.*, 1988], adding capabilities to detect NO_2 by laser-induced fluorescence (LIF) [*Perkins*, 2000] and to detect compounds that can be thermally dissociated to produce ClO, BrO or NO_2, such as $ClONO_2$ [*Bonne*, 1998; *Bonne et al.*, 2000] or $BrONO_2$. The NO_2 subsystem is selective, sensitive, and has the fast time-response (4 Hz) required for observations from an airborne platform, a significant improvement over earlier prototypes [*George and O'Brien*, 1991; *Fong and Brune*, 1997]. In brief, NO_2 is excited by a tunable laser tuned to coincidence with a pair of rovibronic transitions near 585 nm. Fluorescence, red-shifted from the laser wavelength is detected using a Ga:As photomultiplier. During POLARIS this instrument measured the concentration of NO_2 ($[NO_2]^{LIF}$) with an estimated systematic uncertainty of ±10% ±50 parts per trillion by volume (pptv) and an average precision of ±40 pptv for data reported at 10 s intervals. (In the discussion of systematic errors the notation $\pm A\%$ $\pm B$ pptv will be used where A indicates a multiplicative error and B indicates an additive error as would be representative of a zero offset. Throughout the text, uncertainties and error limits will be represented as 1σ.) Details of the design, performance, and calibration of this instrument are described by *Perkins* [2000]. Improvements to the design of the instrument including higher laser power, more sensitive detectors, optical designs that improve the signal rate while simultaneously reducing noise, and operation at reduced pressure are expected to increase the sensitivity by an order of magnitude, making LIF the most sensitive technique available for the observation of NO_2 in the stratosphere [*Perkins*, 2000]. *Thornton et al.* [2000] have implemented some of these changes in an instrument designed for tropospheric measurements from the ground or aircraft. That instrument has a systematic uncertainty of ±10% ±1 pptv with a precision of 15 pptv for data reported at 10 s.

The abundance of NO_2 was also measured during POLARIS by another instrument employing the technique of photolysis followed by detection of NO using $NO+O_3$ chemiluminescence [*Del Negro et al.*, 1999]. This instrument measured the concentration of NO_2 ($[NO_2]^{P\_CL}$) with a systematic uncertainty of ±15–30% and an average precision of ±50 pptv for data reported at 1s sample periods (±16 pptv when averaged to 10s). The $[NO_2]^{LIF}$ and $[NO_2]^{P\_CL}$ measurements are in excellent agreement throughout the POLARIS mission, with a linear fit of the measurements giving $[NO_2]^{LIF} = 1.07 \times [NO_2]^{P\_CL}$ and an R^2=0.95. No improvement in this fit is observed when the intercept is allowed to vary from zero. For the purposes of this analysis, we combine the two data sets by averaging the chemiluminescence measurements to 10s and then splitting the difference between the measurements. We define the observed NO_2 concentration, $[NO_2] = (0.965 \times [NO_2]^{LIF} + 1.035 \times [NO_2]^{P\_CL})/2$ when both measurements are available, and $[NO_2]=0.965\times[NO_2]^{LIF}$ or $[NO_2]=1.035\times[NO_2]^{P\_CL}$ when only one is available. We use ±10% ±50 pptv as an upper limit to the systematic uncertainty for the average $[NO_2]$, equivalent to that reported for $[NO_2]^{LIF}$. In the NO/NO_2 analysis we include only those points where $[NO_2]$ is greater than 500 pptv. In the NO_x/HNO_3 analysis, we include points where $[NO_2]$ is greater than 250 pptv. These selection criteria insure that the observations were obtained in the stratosphere and eliminate the possibility that errors associated with a zero offset affect our conclusions. The stronger constraint used in the NO/NO_2 analysis allows a more precise test than is possible for the NO_x/HNO_3 photochemistry.

2.2. Other In Situ Observations

In addition to NO_2, our analysis uses simultaneous observations of NO, NO_y, OH, HO_2, ClO, $ClONO_2$, O_3, H_2O, N_2O, pressure, temperature, and particle surface area density. The detection technique, reporting interval, systematic uncertainty (1σ), and precision (1σ) for these species are summarized in Table 2. We infer the measurement precision for the reporting interval by analyzing the scatter about a running median filter through the reported flight data. These estimates are representative of the short-term precision of the instruments and are a lower limit on the long-term precision of the measurements which will be influenced by systematic

Table 2. ER-2 in Situ Observations

Species	Detection Technique	Reference	Reporting Interval (s)	Estimated Systematic Uncertainty (1σ)	Precision Uncertainty[a] (1σ)
NO_2	laser-induced fluorescence (LIF)	*Perkins* [2000]	10	±10% ±50 pptv	±40 pptv
NO_2	photolysis/chemi-luminescence(CL)	*Del Negro et al.* [1999]	1	±15 - 30%	±50 pptv
NO	CL	*Fahey et al* [1989]	1	±6% ±4 pptv	±13 pptv
NO_y	catalytic conversion/CL	*Fahey et al.* [1989]	1	±10 ±100 pptv	±80 pptv
OH	LIF	*Wennberg et al.* [1994a]	2	±13% ±0 01 pptv	±0.03 pptv
HO_2	reaction with NO/ LIF	*Wennberg et al.* [1994a]	2	±15% ±0.01 pptv	±0.15 pptv
H_2O	photofragment fluorescence	*Hintsa et al.* [1999]	4	±5%	±0.11 ppmv
ClO	resonance fluorescence	*Bonne* [1998]	35	±15%	±3 pptv
$ClONO_2$	thermal dissociation/ resonance fluorscence	*Bonne* [1998]	35	±20%	±10 pptv
O_3	UV absorption	*Proffitt and McLaughlin* [1983]	1	±5%	±6 ppbv
N_2O^{ATLAS}	laser absorption	*Podolske and Loewenstein* [1993]	1	±2.5%	±1.8 ppb
N_2O^{ALIAS}	laser absorption	*Webster et al* [1994b]	3	±5%	±1.3 ppb
O_3 column over ER-2	spectroradiometer	*McElroy* [1995]	132	± 3%	±1 DU
Pressure	pressure sensor	*Scott et al.* [1990]	1	±0.3 mbar	±0.06 mbar
Surface Area	aerosol spectrometer	*Jonsson et al* [1995]	30	±60%	±0.03 $\mu m^2/cm^3$
Temperature	temperature sensor	*Scott et al* [1990]	1	±0.3 K	±0.25 K

[a] Average precision uncertainty at the reporting interval.

errors that may vary flight-to-flight or over the duration of a flight. All observations are averaged to 10s prior to analysis. For the species reported less frequently ([ClO], [$ClONO_2$], and particle surface area density, [SA]), linear interpolation is used to infer the concentration between measurements. The concentration of HNO_3 is inferred from observations as NO_y – (NO_2 + NO + $ClONO_2$ + $BrONO_2$ + 2×N_2O_5 + HO_2NO_2 + NO_3), where the latter four compounds are inferred from the photochemical calculations described below. The uncertainty in the inferred HNO_3 is approximately 10%.

2.3. Photolysis Rates

The photolysis rate for a chemical species depends on the absorption cross section of the species, the quantum yield for dissociation, and the actinic flux. We calculate local radiative flux using a radiative transfer model [*Prather*, 1981; *Salawitch et al.*, 1994] that has been extensively compared with other codes [*Stolarski et al.*, 1995]. Absorption cross sections and quantum yields are based on the Jet Propulsion Laboratory (JPL) 1997 recommendations [*DeMore et al.*, 1997]. Photolysis rates are calculated at 1 to 5 min intervals along the ER-2 flight track, and linear interpolation is used to infer photolysis rates between these points. At each of these points, the diurnal behavior of the photolysis rates is characterized by running the radiative-transfer model from midnight to midnight at 15-minute intervals. Uncertainty in the photolysis rates is introduced through the calculated actinic flux, the absorption cross sections, and the quantum yields. The radiative transfer model includes the effects of SZA, ozone column above the ER-2 (overhead O_3 measured by CPFM [*McElroy*, 1995]), albedo, cloud height, local temperature and the seasonal variation in the Earth-Sun distance. We find no evidence that the radiative transfer model, when constrained by the CPFM observations, is the dominant source of noise in our analysis. Further, we find no evidence of a bias in the analysis at high SZA where the geometry makes the CPFM measurements most difficult. The analysis is constrained to SZA<85° to reduce the possibility of biases at high SZA

Albedo along the ER-2 flight track is inferred from TOMS reflectivity measurements. In section 3, where we examine the accuracy of NO/NO_2 photochemistry in the photolysis rate calculation, we use the TOMS albedo measured along the flight track as an estimate of the albedo at the location where the ER-2 measurement occurred. The TOMS measurements are not coincident with the aircraft observations, but the small differences that occur over a few hours are expected to average to zero in a large enough sample. The observed partitioning between NO_x and HNO_3 (section 4) will not reflect the albedo at the time of measurement, but rather an "effective albedo" experienced during the last several days. This occurs because the rate of NO_x–HNO_3 exchange depends on the concentration of NO_2 (not on the concentration of NO_x), because the abundance of NO_2 is particularly sensitive to albedo, and because NO_x and HNO_3 establish a diurnal steady state on a timescale of a few days. Air parcel transport history is characterized using the Goddard Space Flight Center (GSFC) Isentropic Trajectory Model. Ten-day back trajectories are calculated for air parcels at 7-min intervals along the ER-2 flight track. Daily TOMS reflectivity data are coupled with these back trajectories to determine the albedo history of the air parcel. We define the "effective albedo" for

the NO_x–HNO_3 system as a weighted average of the albedo along the back trajectory by assuming that the diurnal steady state ratio of NO_x to HNO_3 is established on a timescale equivalent to the lifetime of NO_x and that this ratio will reflect the albedo over the most recent history more strongly than the albedo experienced days prior to observation. Linear interpolation is used to estimate the effective albedo between back trajectory calculations. Photolysis rates used in calculation of $NO_x \Leftrightarrow NO_y$ exchange are calculated using this effective albedo. An average cloud height of 590 mbar is used for these calculations. We have not considered variations in overhead O_3 along the back trajectory. The use of "effective albedo" is discussed further by *Perkins* [2000].

2.4. Photochemical Calculations

In section 4, we use a highly constrained, semiempirical, photochemical model to test our understanding of NO_x/HNO_3 chemistry. The calculation includes the reactions from Table 1, the chemistry coupling the major inorganic bromine species (BrO, $BrONO_2$, and HOBr), and chemistry partitioning ClO and $ClONO_2$. It is constrained by ER-2 observations of OH, O_3, the sum of $ClONO_2$ and ClO, NO_y, H_2O, temperature, pressure, and aerosol surface area in order to isolate the reaction set that affects NO_x/HNO_3 from possible errors in the photochemical rate equations necessary to describe these other species. OH concentrations at any time t are specified from an empirical relationship:

$$[OH]\,(t) = [OH]_0\,(94 - SZA(t))/(94 - SZA_0);$$
$$[OH](t) = 0 \text{ where } SZA(t) > 94,$$

where $[OH]_0$ and SZA_0 are values at the time of the measurement [*Wennberg et al.*, 1994b]. This empirical relationship provides a considerably more precise representation of the observations than a free-running model would. We estimate it captures the diurnal variation to better than 10%. Total inorganic bromine (Br_y) is estimated using measurements of N_2O together with an N_2O–Br_y relationship. We transform the Br_y-CFC11 relationship reported by *Wamsley et al.* [1998] to N_2O using the observed correlation of N_2O with CFC11.

Concentrations of the NO_x radicals and the partitioning of NO_y between NO_x and HNO_3 are determined by integrating the photochemical equations for 20 days. For all of the data used in our analysis, this corresponds to at least 3 times the lifetime of NO_x insuring a good approximation to a diurnal photochemical stationary state (DPSS) solution is achieved (a molecule in DPSS has a concentration that varies with a 24-hour periodicity). The benefits of this highly constrained model are that it allows us to focus on model-measurement discrepancies in the NO_x/HNO_3 ratio while reducing the potential that we are inadvertently transmitting errors from other components of a free running photochemical model (e.g., those that are required to compute OH or the $ClONO_2$-HCl partitioning) to the nitrogen radicals. However, it is important to recognize that as a consequence, the model is much less sensitive to absolute rates. Largely, if all the rates in the model were multiplied by a constant of order 1 to 2, there would be no change in predicted NO_x/HNO_3. In contrast, a model that does not fix OH would likely predict quite different OH abundances in response to such changes. Rate constant changes substantially larger than a factor of 2 would cause a large enough perturbation to the diurnal profile of the model predictions of NO_x that absolute errors in the rate constants would be apparent even in the highly constrained model-measurement comparison presented in this paper.

Calculations were performed with two sets of reaction rate coefficients, one using parameters as given in JPL 1997 and the other using rates for the reaction of $OH+NO_2$ as recommended by *Dransfield et al.* [1999] and that for $OH+HNO_3$ as recommended by *Brown et al.* [1999b]. The latter model is denoted "Rates '99" throughout the text and figures. These rates coefficients are similar to those recommended in JPL 2000 [*Sander et al.*, 2000] which became available after submission of this manuscript.

3. Chemical Coordinates: NO_x Partitioning

Observations show that two distinct timescales affect the abundance of NO_x in the lower stratosphere. The partitioning of NO and NO_2, the focus of this section, occurs on a timescale of minutes. In section 4 we examine the partitioning of NO_y between radicals and reservoir species which occurs on a timescale of days.

3.1. Chemical Coordinate Definition

The reactions

(R20) $NO_2 + h\nu \rightarrow NO + O$
(R16) $NO + O_3 \rightarrow NO_2 + O_2$

typically describe the interconversion between NO and NO_2 in the lower stratosphere to better than 90% [e.g., *Jaegle et al.*, 1994; *Del Negro et al.*, 1999]. Reactions of NO with ClO, BrO and HO_2 make up the remaining 10%.

NO and NO_2 reach a steady state within minutes, if both the solar zenith angle and the albedo are changing slowly. Under these conditions a model describing the coupled NO/NO_2 reaction set is given by equation (1):

$$J_{NO2}\left(\int \sigma(T) I(\nu) d\nu\right)[NO_2] = k_{NO+O3}(T)[NO][O_3] + \Sigma k_{NO+Xi}(T)[NO][X_i]; \quad (1)$$

where X_i = ClO, BrO, HO_2, T indicates that both the absorption cross-section and the rate coefficients depend on temperature, and $\int\sigma(T)I(\nu)d\nu$ indicates the photolysis rate depends on the integral over a product of the absorption cross section and the solar radiation field. The accuracy of this equality is what we intend to evaluate using observations. Rate coefficients for reactions $A+B$ will be denoted k_{A+B} and rate coefficients for photolysis of A as J_A in this text. If this model is complete; that is there is no "missing chemistry," then a comparison of observations to the model provides information about the accuracy of the model and its components.

The model is a function of temperature, the radiation field, NO, NO_2, O_3, ClO, BrO, and HO_2. With the exception of BrO all of these quantities were measured during POLARIS. We choose as the chemical coordinates temperature and the radiation field because these are the fundamental parameters that are used in models to calculate NO_x partitioning. Figure 2 is a plot of the set, $\{T, \int I(\nu)\}$, where POLARIS observations were obtained. We use the CPFM measurements of mean intensity from 325-375 nm scaled by a factor of (1+albedo) as

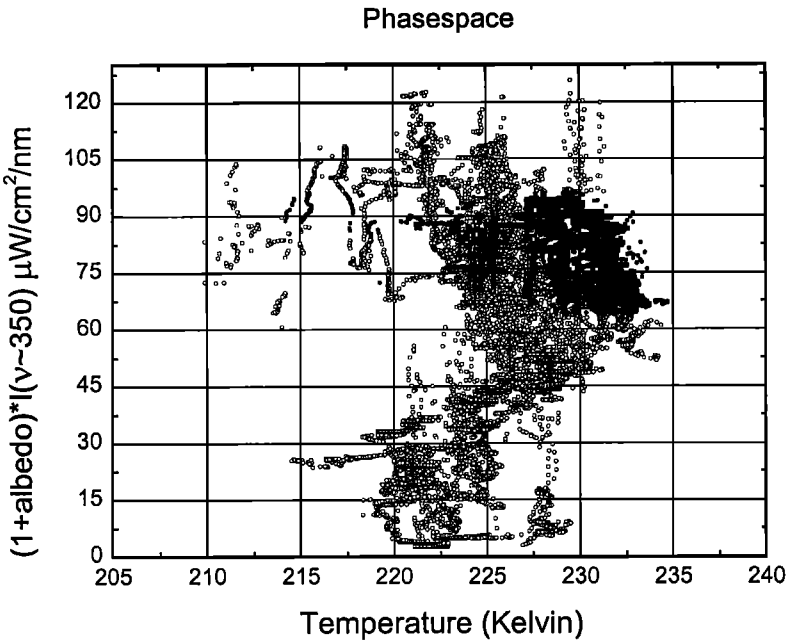

Figure 2. Phase-space of the primary coordinates, temperature and light intensity $\{T, \int I(\nu)\}$, in a model of the NO to NO_2 ratio. The vertical axis is the observed albedo weighted mean intensity from 325-375 nm. Points in gray are all observations at solar zenith angles less than 85° and $[NO_2]$>500 pptv. Points in black are selected from the black set and have albedo=0.7±0.2 and the mean intensity averaged from 325-375nm equal to 80±16 $\mu Wcm^{-2}nm^{-1}$.

an indicator of the integrated radiation field intensity at the wavelengths that dominate NO_2 photolysis.

3.2. Model Evaluation: Accuracy

Rearranging equation (1) to focus attention on quantities that are important and difficult to measure, J_{NO2} and k_{NO+O3}:

$$\frac{J_{NO_2}\left(\int I(\sigma(T)\upsilon)\right)}{k_{NO+O_3}(T)} = \frac{[NO][O_3]}{[NO_2]} + \sum_i \frac{k_{NO+Xi}[NO][X_i]}{k_{NO+O_3}(T)[NO_2]} \quad (2)$$

and recalling that the second term on the right side of equation (2) is small, we see that the ratio, J_{NO2}/k_{NO+O3}, can be determined to reasonable accuracy using observations of NO, NO_2, and O_3. Note, however, separate determination of the absolute accuracy of either J_{NO2} or k_{NO+O3} is not possible using atmospheric measurements alone unless the second term on the right side of equation (2) becomes much larger than 10%. In the discussion that follows, we refer to the left side of equation (2) as J_{NO2}/k_{NO+O3}(calculated) and the right side as J_{NO2}/k_{NO+O3}(observed) although the actual separation is not as clean, since observations of albedo, the ozone column, and temperature contribute to J_{NO2}/k_{NO+O3}(calculated).

The absolute accuracy of J_{NO2}/k_{NO+O3}(observed) can be estimated as the weighted root sum of squares (RSS) of the absolute uncertainties of each of the individual terms required to compare the model to observations. The contribution of the primary terms is 11.4%, the RSS of ±6%, ±10%, and ±5% uncertainty in the NO, NO_2 and O_3 respectively, weighted by 0.9. The second term contributes an additional 5% from the combined uncertainty in the rate coefficients for the reactions of ClO and BrO with NO and the concentration of ClO and BrO, weighted by 0.1. A thorough weighted analysis for this system is derived by *Harries* [1982]. Experimental contributions to uncertainty in J_{NO2}/k_{NO+O3}(calculated), include ±10% from the propagation of uncertainty in the radiation field measurements into a value for J_{NO2}, and ±1% for the effect of uncertainty in the measured temperature on the $NO+O_3$ rate coefficient. The total experimental contribution to the uncertainty in the model represented by equation (2) is ±16%, assuming that the model is complete. This error limit is substantially smaller than we can place on either J_{NO2} (~40%) or k_{NO+O3} (~25%) separately, since the large uncertainty associated with laboratory measurements of the $NO+O_3$ rate constant propagate into uncertainty on J_{NO2} and vice versa. The 16% experimental uncertainty is a significant constraint, since the uncertainty in the quantity J_{NO2}/k_{NO+O3} is more than 30% based on the JPL 1997 interpretation of laboratory measurements as ±20% for J_{NO2} and +36%/-26% for k_{NO+O3} at 225K [*DeMore et al.*, 1997] and assuming the uncertainties for the different rate coefficients described by the JPL compendium are independent.

The comparison of J_{NO2}/k_{NO+O3}(calculated) and J_{NO2}/k_{NO+O3}(observed) is shown in Figure 3 along with error limits that reflect uncertainties in estimates of J_{NO2}/k_{NO+O3} derived from observations (gray lines) and the JPL uncertainties at 225 K (black lines). We include all the POLARIS observations with NO_2 > 500 pptv and solar zenith angles greater than 85° in this comparison (15,457 observations out of a total 24,343 observations during the campaign meet this criterion). The temperature-dependent uncertainty is computed using an estimate of ±10% for the uncertainty at room temperature and ±1.7 kJ/mol for the uncertainty in the activation energy. The JPL panel recommends using these parameters to construct a

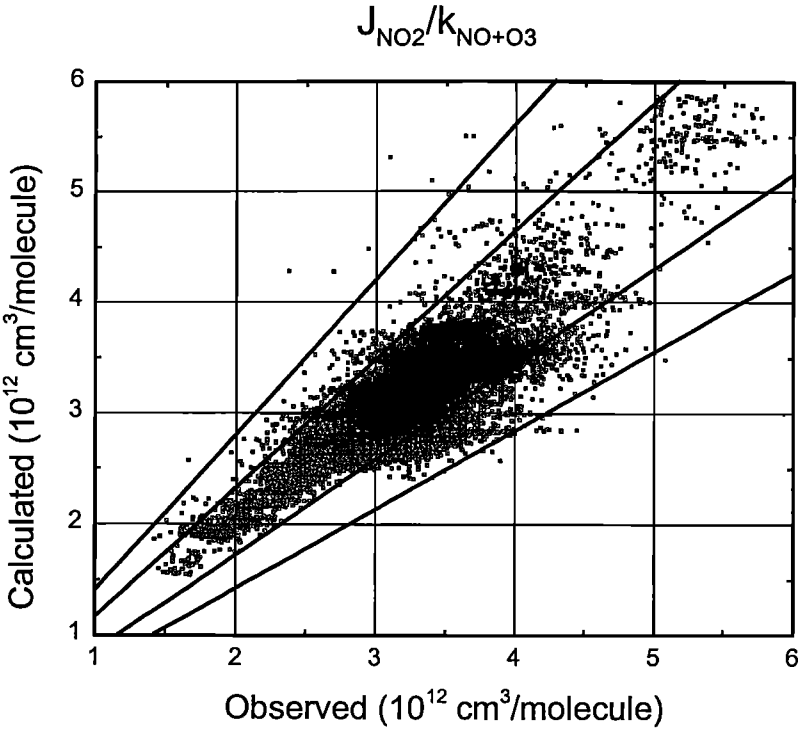

Figure 3. Comparison of observed and calculated J_{NO2}/k_{NO+O3}. The data selection is as described in Figure 2. The inner pair of lines are 16% experimental error bars, and the outer pair are 40% error bars based on the JPL 1997 recommendation for uncertainty in J_{NO2} and k_{NO+O3} at 225 K.

multiplicative uncertainty factor f as $f(T) = 1.1\times \exp\{\{1.7/R\}\times\{1/T\text{-}1/298\}\}$; $f(T)\times k$ and $k/f(T)$ are then estimates of the value of the rate coefficient at the 1σ uncertainty bounds [*DeMore et al.*, 1997].

The mean difference between the left and right sides of the model:

$$100\times\frac{J_{NO2}/k_{NO+O3}(\text{obs})-J_{NO2}/k_{NO+O3}(\text{calc})}{J_{NO2}/k_{NO+O3}(\text{obs})} \quad (3)$$

is +2.6% (not shown in the figure). The small difference indicates the quantity J_{NO2}/k_{NO+O3} is indeed accurate at current values, at least at the temperature and actinic flux typical of the POLARIS experiment. This conclusion about the calculated ratio J_{NO2}/k_{NO+O3} is similar to that arrived at by *Del Negro et al.* [1999] who report comparisons of observed and calculated J_{NO2} using POLARIS data ranging from 1 to 14% depending on the choice of the source of the radiation field and in contradiction to the results of *Jaegle et al.* [1994] and *Sen et al.* [1998] who report much larger model-measurement discrepancies. (Note since the analysis in this paper makes use of an expanded data set from both NO_2 instruments, each adjusted by 3.5% there are slight numerical differences between our results and those reported by *Del Negro et al.* even for otherwise identical comparisons.)

3.3. Model Evaluation: Temperature Dependence

Analysis of the absolute accuracy of the model treats each observation as if it were independent from the other observations. However, in most atmospheric measurement campaigns and certainly during POLARIS, a large suite of observations is collected and the error in these observations has a high degree of covariance. Typically, the observations are precisely calibrated, such that a single multiplicative constant and/or offset represents most of the (systematic) uncertainty and the remaining variance in calibration factors is small. Precisely calibrated observations can be used to constrain crucial aspects of the model, in the example here, the first derivative with respect to temperature or with respect to the radiation field much more accurately than they can be used to define the absolute accuracy of the model.

To illustrate the point, we use NO_2 in the following example of interpreting an instrument calibration factor, C(t), that relates the measured abundance of NO_2, or any other species, to the true value [*Thornton et al.*, 2000]:

$$[NO_2]^{measured} = C(t)[NO_2]^{true} + Zero(t) \quad (4)$$

and

$$C(t) = C_0 C_{adjustments}(t) C_{drift}(t) C_{random}(t) \quad (5)$$

The measured value of NO_2 is equal to the true NO_2 when $C(t)$ is equal to 1 and zero(t) is equal to zero. The temporal dependence of $C(t)$ is divided into four parts: C_0, represents the time-invariant calibration. For NO_2 measurements by LIF, uncertainties in this term includes the temperature dependence of the NO_2 fluorescence signal, the concentration of the calibration standard and related factors that could be better determined by laboratory experiments. C_{random} represents the finite precision of the instrument. Averaging any subset of identical measurements will improve the precision of the measured concentration by bringing C_{random} closer to a value of 1. The other two components of the calibration represent

factors that are time-varying. C_{drift} describes factors that vary slowly and continuously such as might occur if the laser alignment, or transmission bandpass of the optical filters used were slowly degrading, or if the concentration of the calibration standard were changing. $C_{adjustments}$ describes systematic changes to the instrument that result from operator intervention such as might be associated with aligning a laser or in a photolysis-chemiluminescence experiment cleaning the chemiluminescence cell.

For the purposes of this analysis, we define precisely calibrated measurements as those for which (1) systematic error in the observations is weakly dependent (or independent) of the chemical coordinates and (2) the change in systematic error on the time scale of the measurement campaign is small. This is true for all of the observations used in this analysis. Precise calibration is not to be confused with precise measurements. We assume that repetitive observations at a point in the chemical phase-space provide statistical information about the precision of the observations at that point and can be averaged, reducing the random errors to a negligible fraction of the total error, that is bringing C_{random} closer to 1. For instruments whose calibration is adequately represented by equations (4) and (5), a test of the temperature dependence of a model, or of terms in a model such as represented by the left side of equation (2), can be more accurate than a test of the absolute accuracy because the measurement error is not a function of temperature. For example, while the uncertainty that NO_2 measurements contribute to assessment of the absolute accuracy in the ratio J_{NO2}/k_{NO+O3} is ±10%, one of the larger contributions to the error budget, the uncertainty these same measurements contribute to assessment of the accuracy of the temperature dependence in J_{NO2}/k_{NO+O3} is negligible.

In addition to precise and precisely calibrated measurements, a useful test of the model also requires that we sample over a wide range in the chemical phase space, in this case $\{T, \int I(\nu)\}$. Thus the large majority of points (Figure 2) in the range 45-90 $\mu Wcm^{-2}nm^{-1}$, 225-230 K are essentially redundant measurements that provide insight into the combined precision of our observational methods and techniques for inferring the photolysis rates. By contrast, the chemical information contained in the few points at 90 $\mu Wcm^{-2}nm^{-1}$, 210-220K is unique in this data set.

To illustrate the utility of a chemical coordinate analysis, we first examine the accuracy of the model represented by equation (2) as a function of temperature. Knowledge of the temperature dependence of the NO_2/NO ratio is particularly important since a considerable body of literature is built on inferences of NO_2 from measurements of O_3, NO, and temperature and the assumption that the photochemistry represented by equation (2) is accurate. To evaluate the temperature dependence, we restrict the comparison to observations where NO_2 is greater than 500 pptv, SZA<85°, the albedo weighted 350 nm integrated radiation field is 80 ± 16 $\mu Wcm^{-2}nm^{-1}$ and the albedo is 0.7 ± 0.2 (of the 15,457 measurements that meet the NO_2 and solar zenith angle criteria, 4747 meet the radiation field criteria). The restrictions on the parameters that control the radiation field reduce the possibility that errors in the radiation model that are correlated with temperature will bias our ability to evaluate the temperature dependence of J_{NO2}/k_{NO+O3}. Observations that meet these criteria are shown as gray circles on Figures 2-5.

By holding the parameters that affect the radiation field constant, this analysis is equivalent to comparing the partial derivatives of the left- and right-hand sides of the model with respect to temperature at constant radiation field as indicated

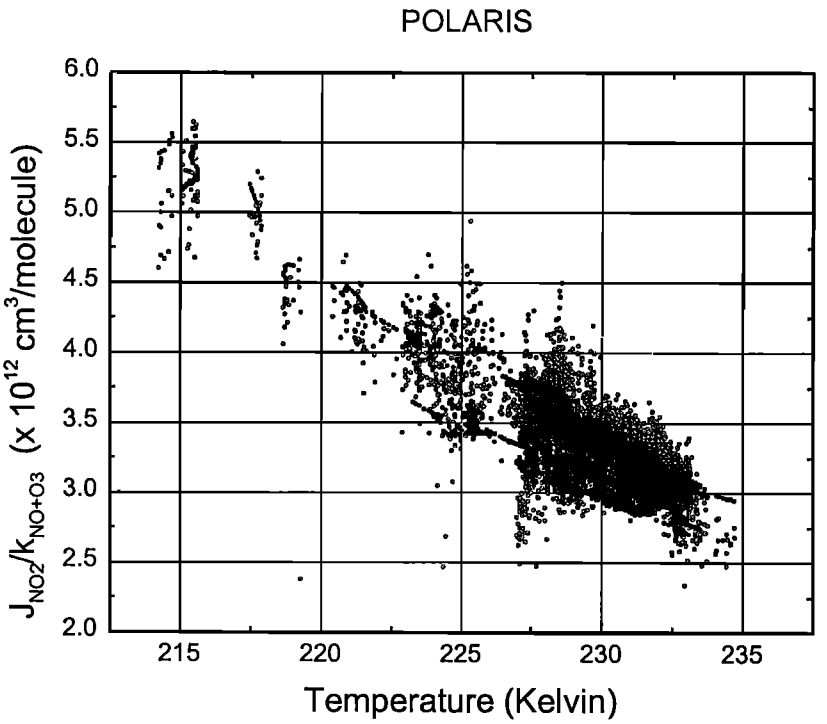

Figure 4. The observed (black) and calculated (gray) ratio, J_{NO2}/k_{NO+O3}, versus temperature at a constant value of the light field (albedo=0.7±0.2 and the mean intensity averaged from 325-375 nm equal to 80±16 $\mu Wcm^{-2}nm^{-1}$).

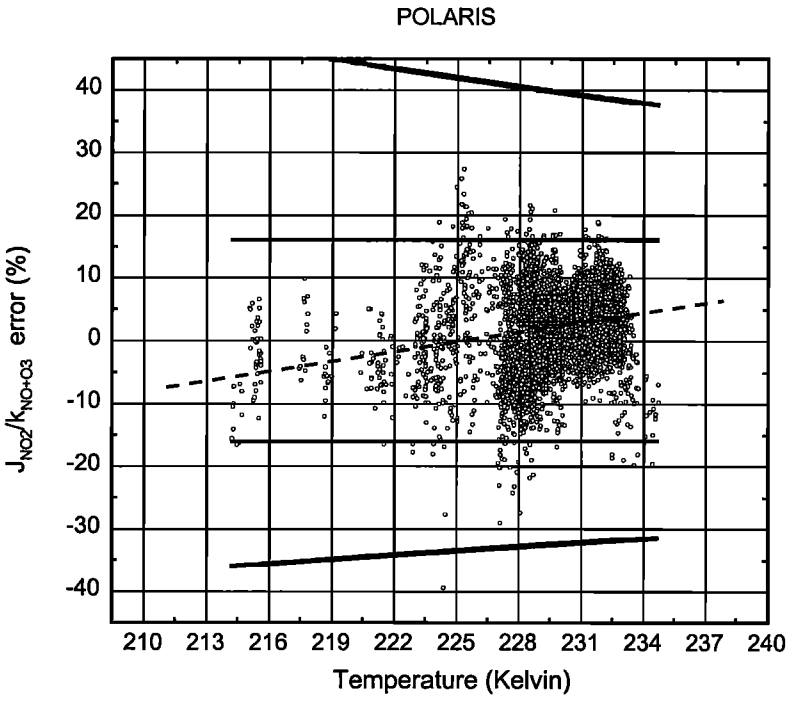

Figure 5. Percentage error in J_{NO2}/k_{NO+O3} versus temperature at a constant value of the light field (see Figure 2 or 4). The dashed line is a fit to the points shown. The inner pair of horizontal lines are the experimental uncertainty in J_{NO2}/k_{NO+O3} and the outer pair are the temperature-dependent uncertainty in calculated values of J_{NO2}/k_{NO+O3} estimated using the JPL 1997 prescription.

in equation (6):

$$\left.\frac{\partial\left(\frac{J_{NO_2}(T,\int I(\nu))}{k_{NO+O_3}(T)}\right)}{\partial T}\right|_{\int I(\nu)} = \left.\frac{\partial\left(\frac{[NO][O_3]}{[NO_2]}+\sum_i \frac{k_{NO+X_i}[NO][X_i]}{k_{NO+O3}(T)[NO_2]}\right)}{\partial T}\right|_{\int I(\nu)} \quad (6)$$

Figure 4 shows a plot of the argument of the differential operators in equation (6). The calculated values of J_{NO2}/k_{NO+O3} are shown in black, and the J_{NO2}/k_{NO+O3} inferred from observations are shown in gray. The steep temperature dependence is due to the high activation energy of the NO + O_3 reaction. The rate of this reaction is about 50% faster at 230 K than at 215 K. The terms associated with halogen oxides and HO_2 reactions with NO change quite slowly with temperature by comparison to the NO + O_3 reaction because their rate coefficients have a low activation energy, because they are small throughout the POLARIS data set, and because the concentrations of these species were only weakly correlated with temperature during these flights. The temperature dependence of J_{NO2} is also quite small, approximately 0.04%/K. Therefore we can neglect the contribution of the temperature dependence in these terms to the overall temperature dependence of the photochemical model.

The steep temperature dependence hides any subtle errors in the comparison between the two routes to determining J_{NO2}/k_{NO+O3}. The implications of the comparison shown in Figure 4 are easier to discern if we evaluate equation (3) at constant actinic flux and plot the percentage difference between observed and calculated J_{NO2}/k_{NO+O3} as a function of temperature. This comparison is shown as the gray circles in Figure 5 along with a linear least squares fit to data used in the comparison (gray line). The model-measurement comparison uses the JPL 1997 recommendation for the rate of NO+O_3: $k_{NO+O3}= Ae^{-Ea/(RT)}$, $A= 2x10^{-12}$, E_a=11.7 kJ/mole. The comparison shown along the chemical coordinate (temperature) is acceptable if (1) the points lie between the experimental error limits (inner pair black lines at ±16%) and (2) a line fit to the model-measurement comparison has a slope near zero.

The comparison of the J_{NO2}/k_{NO+O3} using JPL 1997 recommendation has a slope along this chemical coordinate indicating a temperature dependent error of 0.52%/K, with a statistical uncertainty of 0.03 K. The outer pair of black lines shown in Figure 5 are the JPL 1997 temperature dependent uncertainty in the ratio, J_{NO2}/k_{NO+O3}. While the absolute model error is small compared the JPL 1997 error, the temperature-dependent error (the slope) is comparable to the temperature dependent uncertainty (similar slopes) in the JPL 1997 recommendation. This is consistent with the conclusions of *Del Negro et al.* [1999] who fit all the data without isolating for constant radiation field and concluded a 0.7%/K error was present in the model-measurement comparison. As can be seen from the range of phase space sampled during POLARIS (shown in Figure 2), the bulk of the information outside the 220-230 K range is at the light intensity we selected to hold constant, 80 $\mu Wcm^{-2}nm^{-1}$. *Del Negro et al.'s* analysis is strongly influenced by this data because it is the bulk of both the low and high temperature data used in their evaluation. Thus it is not surprising the two analyses produce similar results. However, we note that the numerical values of the

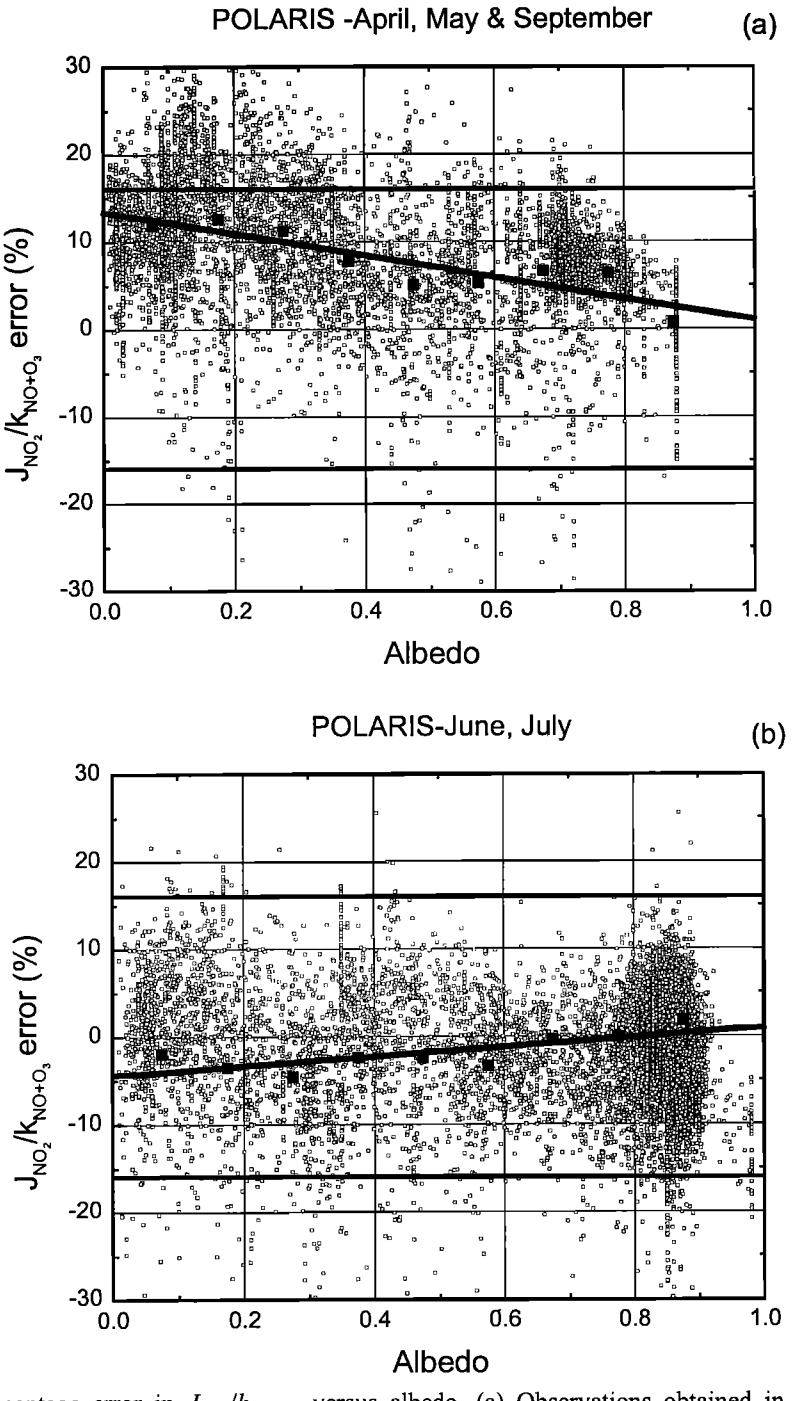

Figure 6. Percentage error in J_{NO2}/k_{NO+O3} versus albedo. (a) Observations obtained in April, May and September. (b) Observations from June and July. Black squares are the average value over a range in albedo of 0.1. The central line is a fit to the points; the outer pair is the experimental uncertainty.

errors identified are not independent of the choice of albedo. If we fix the albedo at 0.2±0.2, the slope error is 1.37%/K. The correlation of errors in temperature with albedo is indicative of an additional error in the model and of the need for more extensive sampling of the phase space at low temperature.

3.4. Model Evaluation: Albedo Dependence

The primary inputs to the radiation calculation are the overhead ozone and the albedo. Since *Perkins* [2000] shows that photolysis rate calculations using CPFM overhead ozone are precise and because of the coupling of the temperature-dependent error to choice of albedo, we chose albedo as a second chemical coordinate. Figure 6 shows the percentage difference between calculated and observed J_{NO2}/k_{NO+O3} as a function of albedo for separate observing periods. Figure 6a shows observations obtained in April, May, and September, and Figure 6b observations from late June and early July. The spring and fall data evidence an error associated with albedo (the slope of the data along this chemical coordinate is

nonzero) of 12.5%, while the summer data have a smaller error (5%) of opposite sign. We do not understand the mechanism responsible for these errors, although it seems likely that the radiation model is systematically underestimating the albedo during spring and fall and overestimating, by a smaller extent, during summer. An empirical fix of $J_{NO2}=J_{NO2}(1.125\text{-}0.125 \times \text{albedo})$ for the data in the spring and fall and $J_{NO2}=J_{NO2}(0.96+0.04 \times \text{albedo})$ for data obtained during the summer renders the analysis essentially uniform across the seasons with respect to albedo. Since the seasonal albedo error is small at high albedo, the effect of this change on our conclusions about the temperature dependent error at high albedo is small. The error in J_{NO2}/k_{NO+O3} determined using a data set corrected as indicated is 0.46%/K JPL 1997 for an albedo of 0.7±0.2. At an albedo of 0.2±0.2 the error is 0.76%/K. While it is reassuring that this empirical correction for the seasonal error in the radiation field brings the temperature-dependent error closer to being independent of albedo, slices through the data set at different temperatures indicate that the error is not the same for all observations in a given season. Without improved understanding of the albedo error, or a more extensive data set at low temperature, we estimate the uncertainty in our derivation of the temperature dependence of k_{NO+O3} as the difference between these two numbers, 0.3%/K.

3.5. NO_x Partitioning-Summary

The 0.46(±0.3)%/K slope indicates that the temperature dependence of k_{NO+O3} is too steep. This result is consistent with laboratory experiments that indicate the effective activation energy for the $NO+O_3$ reaction in the 215-235 K range is lower than recommended by JPL 1997. As discussed by *Borders and Birks* [1982], this might be because two processes, one with a low barrier to produce NO_2 in its ground electronic state and another with a higher barrier leading to an electronically excited NO_2 product are occurring simultaneously. A fit to a single exponential gives an activation energy biased high because of the process leading to excited state NO_2. In Figure 7 we compare a number of laboratory measurements of the rate of the $NO+O_3$ reaction to the JPL 1997 recommendation for the reaction rate coefficient (gray symbols). We also show a comparison to other inferences of J_{NO2}/k_{NO+O3} from atmospheric observations (black symbols). So that the inferences about k_{NO+O3} are of the same form as the J_{NO2}/k_{NO+O3} derived from the atmosphere, we show the comparison as the percentage error in $1/k_{NO+O3}$. Measurements shown with triangles support a shallower activation energy at these temperatures, measurements shown as squares or circles are consistent with the JPL 1997 activation energy, and measurements shown as stars are too imprecise or too few to provide insight. Observations by *Moonen et al.* [1998] at 200 K and by *Sen et al.* [1998] at 209 and 215 K are too far from the JPL 1997 value to show in this figure -56%, -117%, and –72%, respectively. We also note that the JPL 2000 recommendation released after the initial submission of this manuscript increased the activation energy for the $NO+O_3$ reaction by 7% [*Sander et al.*, 2000]. This will increase the discrepancy between models and observations of the partitioning of NO_x at low temperature.

The rate expression of *Borders and Birks* [1982], $k_{NO+O3}=AT^n e^{-Ea/(RT)}$ A=8.9e-19, n=2.2 E_a= 7.5 kJ/mol is one approach to producing a rate constant with a shallower temperature dependence than the Arrhenius form used by JPL 1997. Using this rate expression we find the temperature dependent error is reduced by almost half to 0.28%/K at high albedo, again with a statistical uncertainty of 0.03 K. This is now within our

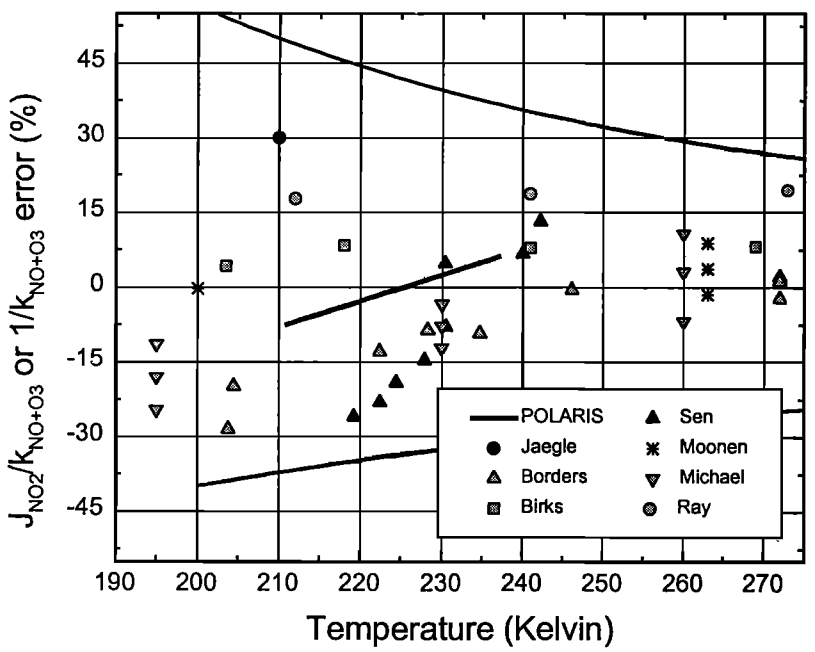

Figure 7. Percentage error in J_{NO2}/k_{NO+O3} and in $1/k_{NO+O3}$ versus temperature. The line in the center of the figure represents the POLARIS measurements. Laboratory measurements, shown as gray symbols, are from *Birks et al.* [1976], *Ray and Watson* [1981], *Michael et al.* [1981] *Borders and Birks* [1982], *Moonen et al.* [1998]. Only measurements below 273K are shown. Atmospheric observations (Black symbols) are from *Jaegle et al.* [1994] and *Sen et al.* [1998]. The outer lines reflect the JPL 1997 estimate of error in *J*/*k*. The error in $1/k$ dominates below 240 K.

estimate of the possible systematic uncertainties (±0.3%/K) in the analysis. Nearly equivalent results could be obtained using a rate coefficient of the Arrhenius form with A= $9x10^{-13}$ and E_a=10kJ/mol, although this a rate expression would be less satisfactory at temperatures above 298 K where the JPL 1997 expression systematically underestimates laboratory observations of the rate coefficient. Using the Borders and Birks rate coefficient and correcting for the albedo error as above, the temperature-dependent error is 0.23%/K and 0.46%/K at albedo of 0.7±0.2 and 0.2±2, respectively. These two changes also reduce the RMS deviation of linear fit of J_{NO2}/k_{NO+O3}(calculated) to J_{NO2}/k_{NO+O3}(observed) from $3x10^{11}$ to $2x10^{11}$ and increase the R^2 of the fit from 0.7 to 0.8. The improvement in these diagnostics of the quality of the model suggests that these changes to the albedo and temperature dependence of the model do accurately capture factors that contribute to atmospheric variance in NO_x partitioning.

It would be equally consistent with the observations to assume k_{NO+O3} is perfect at the JPL 1997 recommendation and to assign all of the error to the temperature dependence of J_{NO2} or to assume that the temperature-dependent error is due to the contribution of missing chemistry. However, a factor of 10 error in the temperature dependence of the NO_2 photolysis would be necessary to describe the data if the $NO+O_3$ rate coefficient were accurate. This is extremely unlikely. For missing chemistry to affect the ratio J_{NO2}/k_{NO+O3} derived from the observations, the product of the reaction rate coefficient and the concentration of the molecule converting NO to NO_2 must be of order 10^{-3}. If the rate coefficient were gas kinetic, $\sim 10^{-10}$, then the missing reactant must have a concentration of approximately 10^7 molecules/cm^3 or a mixing ratio of about 6 pptv. At the same time, for this rate to change by 15% of the $NO+O_3$ rate over the range 215-230 K it requires an activation energy near 10 kJ/mol. Since the combination of a near gas kinetic rate and high activation energies is nearly impossible, the missing reagent must have a still higher abundance if it is to explain the temperature-dependent error.

4. Chemical Coordinates: Application to NO_x/HNO_3

4.1. Chemical Coordinate Definition

The large number of reactions involved in transformations between NO_x and HNO_3 in the stratosphere make the process of defining chemical coordinates for describing the NO_x/HNO_3 ratio more cumbersome than for NO and NO_2. Below 21 km the light initiated reactions:

(R1) $HNO_3 + OH \rightarrow H_2O + NO_3$

(R2) $HNO_3 + h\nu \rightarrow OH + NO_2$

(R3) $N_2O_5 + h\nu \rightarrow NO_2 + NO_3$

(R8) $NO_2 + OH \xrightarrow{M} HNO_3 + M$

control the net daytime photochemistry. At night, NO_x is consumed in the reaction pair

(R21) $NO_2 + O_3 \rightarrow NO_3 + O_2$

(R11) $NO_2 + NO_3 \xrightarrow{M} N_2O_5$.

For the conditions of the POLARIS experiments the rate-limiting step in this couplet is (R21), leading to NO_3 formation. This process occurs during the day, but NO_3 is photolyzed rapidly, inhibiting daytime formation of N_2O_5. Throughout both day and night, N_2O_5 is hydrolyzed on aerosol

(R13) $N_2O_5 + H_2O_{(l)} \rightarrow 2HNO_3$.

The photolysis and reformation of the halogen and peroxy nitrates are rapid reactions that contribute to the cycling of NO_x between radicals and reservoirs:

(R4) $ClONO_2 + h\nu \rightarrow ClO + NO_2$, $Cl + NO_3$

(R5) $BrONO_2 + h\nu \rightarrow BrO + NO_2$, $Br + NO_3$

(R6) $HO_2NO_2 + h\nu \rightarrow HO_2 + NO_2$; $NO_3 + OH$

(R9) $NO_2 + ClO \xrightarrow{M} ClONO_2$

(R10) $NO_2 + BrO \xrightarrow{M} BrONO_2$

(R12) $NO_2 + HO_2 \xrightarrow{M} HO_2NO_2$

but have little net effect on NO_x concentrations. In contrast, the reactions $ClO+NO_2$ and $BrO+NO_2$ when followed by heterogeneous reaction of the halogen nitrates:

(R14) $BrONO_2 + H_2O_{(l)} \rightarrow HOBr + HNO_3$

(R15) $ClONO_2 + H_2O_{(l)} \rightarrow HOCl + HNO_3$

contribute to net NO_x loss. Cycles terminating in $ClONO_2$ hydrolysis are not important to this analysis because of the warm temperatures characteristic of the summer stratosphere. $BrONO_2$ hydrolysis contributes about 5% to NO_x conversion to HNO_3. To simplify the discussion below, we refer to the terms corresponding to (R14) and (R15) as O(5%). These reactions are explicitly included in the detailed model and in all of the figures that follow.

Five reactions dominate the interconversion between NO_x and HNO_3. Production of NO_x occurs by photolysis of HNO_3 and N_2O_5 and by reaction of HNO_3 with OH. Loss of NO_x occurs by reaction of NO_2 with OH and by the nighttime reaction of NO_2 with O_3. At 20 km the NO_x lifetime is usually 2-8 days. Since the bulk of stratospheric flow is zonal, most of the time NO_x should be in a diurnal photochemical stationary-state. If the DPSS condition is satisfied, the 24-hour integrated production will be exactly balanced by the 24 hour integrated loss.

$$\int_{daylight} k_{OH+HNO3}[OH][HNO_3]dt + \int_{daylight} J_{HNO3}[HNO_3]dt + 2\int_{daylight} J_{N2O5}[N_2O_5]dt = \int_{daylight} k_{OH+NO2}[OH][NO_2]dt + 2\int_{night} k_{NO2+O3}[NO_2][O_3]dt + O(5\%). \quad (7)$$

We assume N_2O_5, which has a shorter lifetime than NO_x, is in DPSS, as well,

$$\int_{night} k_{NO2+O3}[NO_2][O_3]dt = \int_{24hours} k_{N2O5+H2O}[N_2O_5][SA]dt + \int_{daylight} J_{N2O5}[N_2O_5]dt. \quad (8)$$

Substituting the right side of Equation 8 into Equation 7 and canceling like terms transforms Equation 7 to:

$$\int_{daylight} k_{OH+HNO_3}(T,[M])[OH][HNO_3]dt + \int_{daylight} J_{HNO_3}(T,I(\upsilon))[HNO_3]dt =$$
$$\int_{daylight} k_{OH+NO_2}(T,[M])[OH][NO_2]dt + \quad (9)$$
$$2\int_{24\,hours} k_{N_2O_5+H_2O}(T)[N_2O_5][SA]dt + O(5\%)$$

Equation (9) shows explicitly the dependency of the rate coefficients on temperature, number density of air ([M]), and the radiation field. The two dominant NO_x loss reactions both lead to production of HNO_3 and the two dominant NO_x production mechanisms are reactions involving HNO_3.

The complexity of equation (9) makes it difficult to derive an equation that separates the components of the model describing NO_x/HNO_3 that are computed or based on laboratory measurements from quantities measured in the atmosphere as cleanly as equation (2) does for a model describing NO_x partitioning between NO and NO_2. Equation (9) explicitly recognizes six coordinates: temperature, [M], [SA], [OH], $\int I(\nu)$, and $[N_2O_5]$ for comparison of models and measurements of the NO_2 to HNO_3 ratio. Also implicit are factors affecting NO_x partitioning between NO and NO_2 (see section 3); affecting the rate of N_2O_5 formation (temperature, NO_2 and O_3); and affecting the balance between N_2O_5 photolysis and hydrolysis (aerosol surface area, the radiation field, and temperature). If we were able to collect arbitrarily large amounts of data spanning the entire range of parameters controlling the abundance of NO_x, we would evaluate the accuracy of the model in the phase space of six-dimensional chemical coordinates defined by these explicit variables. The analysis would proceed stepwise by holding five parameters constant and comparing the model and measurements over a range in the sixth parameter. However, the data are too sparse, and the correlations within the atmosphere too strong to allow complete separation of variables. We are also limited by the absence of observations of HNO_3 and N_2O_5. Observations of N_2O_5 would provide a direct test of equation (8).

Instead of testing our understanding of NO_x/HNO_3 in these primary coordinates, we define two aggregate coordinates that project the points from the six-dimensional phase space onto a plane that emphasizes the essential aspects of the chemical transformations. These coordinates are (1) the percentage of the total NO_x production (the left side of equation (9)) that is due to HNO_3 photolysis and (2) the percentage of the total NO_x loss (the right side of equation (9)) that is due to reaction of OH with NO_2. While there is no guarantee that the coordinates so defined are orthogonal (or that the original six coordinates were either), they have the advantage of having a direct connection to reaction rates that are observable in the laboratory, and they are important coordinates for describing the variations in NO_x abundance that are driven by season, latitude, volcanic eruptions, and other geophysical variables that influence the region of the chemical phase space sampled by the atmosphere. In addition, these coordinates have reduced sensitivity to systematic errors in the measurements of HNO_3 and NO_2 because of the appearance of these quantities in both the numerator and denominator of the respective coordinates. We recognize the ad hoc nature of this particular choice of coordinates and welcome examination of NO_y chemistry along other coordinates.

The locations of measurements from POLARIS in this photochemical phase space (Figure 8) were calculated using the procedure described in section 2. We show two sets of model results, one using the JPL 1997 rate coefficients and the other the rates '99 model. In order not to bias the statistical properties of the data set with essentially redundant measurements, data from the so called "diurnal flights" where the ER-2 flew in a racetrack pattern designed specifically to follow the evolution of an air parcel through 6 hours (970430, 970509, 970911, 970914, 970915, and 970919) are excluded from the analysis. Of the 24,343 measurements, this requirement and the requirement that $[NO_2]$>250 pptv reduce the number of points to 11,286 available for the model-comparison. We use a weaker constraint on NO_2 (NO_2 > 250

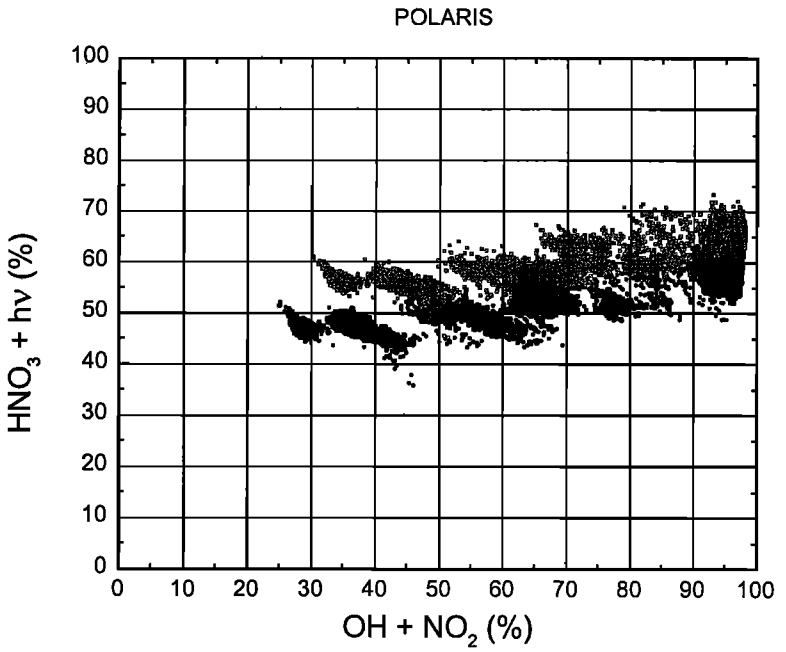

Figure 8. Phase space of parameters sampled for evaluation of NO_x-HNO_3 exchange during POLARIS. Gray points are calculations using the JPL 1997 rates; black are calculated using rates '99. There are 5928 observations shown.

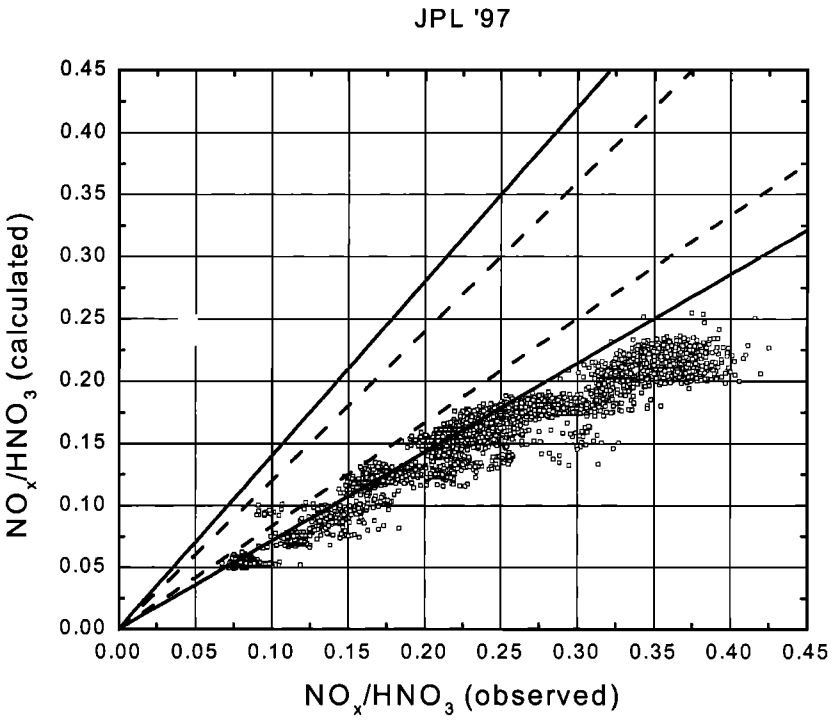

Figure 9. Observed and calculated (JPL 1997) NO_x/HNO_3. The dashed lines are a range about the 1:1 line that corresponds to the experimental error, and the black lines correspond to a minimum estimate of the a priori uncertainty in NO_x/HNO_3 using uncertainty estimates in the parameters from JPL 1997.

pptv instead of 500 pptv) because we are not attempting to diagnose as subtle an error in the model as in the NO/NO_2 analysis. To eliminate noise in the analysis due to air parcels that have not been at the same latitude for long enough to achieve a DPSS, we restrict the sample to those observations where NO_x/HNO_3 DPSS solution computed along 10-day back trajectories varied by less than 20% over the lifetime of NO_x. This constraint reduces the data set to the 5928 points shown in Figure 8. During POLARIS we sampled air with a wide range in the NO_x loss coordinate (30-98%), but only a very narrow range in the NO_x production coordinate (45-65%). High values along the $OH+NO_2$ axis were part of the POLARIS objective and were observed during polar summer where formation of N_2O_5 is inhibited by continuous sunlight. A wide range in the NO_x production coordinate is much more difficult to achieve because it requires extensive sampling in the tropics or at higher altitude.

4.2. Model Evaluation-Accuracy

Analysis of the continuous sunlight observations are the subject of detailed discussion by *Gao et al.* [1999] and *Perkins* [2000]. The chemical coordinates provide a context for smoothly and continuously connecting these observations to those obtained in air masses where N_2O_5 hydrolysis is an important NO_x sink. In Figure 9 we show calculated (JPL 1997) and observed NO_x/HNO_3. The model and the calculation exhibit a mean deviation of 33.5%. The two solid gray lines represent the experimental uncertainty of ±20%; nearly every observation is outside this range. The solid black lines represent a lower limit of 40% on the uncertainty in the calculated NO_x/HNO_3 derived by assuming ±30% uncertainty in the rate coefficients for the NO_x production reactions and for the $OH+NO_2$ reaction and neglecting all other uncertainty. For conditions where N_2O_5 hydrolysis is dominant, an estimate of the uncertainty is much larger since the JPL 1997 recommendation for uncertainty in the rate of N_2O_5 hydrolysis is $\times\div 2$. Given these large uncertainties, it is not surprising that the calculations and measurements differ. In fact, what is more surprising is that photochemical calculations reproduce these and other observations [e.g., *Cohen et al.*, 1994] much more accurately than any propagation of the uncertainties would suggest is reasonable. In the rates '99 model (not shown) the mean difference is reduced to 10.5%. This is consistent with the conclusions of recent studies by *Gao et al.* [1999] and *Osterman et al.* [1999].

4.3. Model Evaluation: NO_x Sinks

By analogy to Figure 4, the observations and the JPL 1997 model of NO_x/HNO_3 are plotted as a function of the chemical coordinate, percent NO_x loss by the reaction $OH+NO_2$, in Figure 10. The observations and calculations shown were selected to have a constant value in the $HNO_3+ h\nu$ chemical coordinate by requiring the points chosen (3494) to be within one standard deviation, ±4.4%, of the mean along this coordinate (60.5%). Observations were obtained at values of NO_x/HNO_3 ranging from 0.075 to 0.4. The variation in the observed ratio reflects the decrease in the ratio of NO_x production to loss under conditions where N_2O_5 hydrolysis is dominant. In Figure 11, by analogy to Equation 3 and Figure 5 we show the percentage error of the model-measurement comparison as a function of the percent loss by $OH+NO_2$ chemical coordinate. Again, we hold the position along the $HNO_3+ h\nu$ chemical coordinate constant. For the rates '99 model the mean and 1σ range in this coordinate is 52.1%±5.5% (3581 points are with 1σ of the mean).

As discussed above, a model-measurement comparison

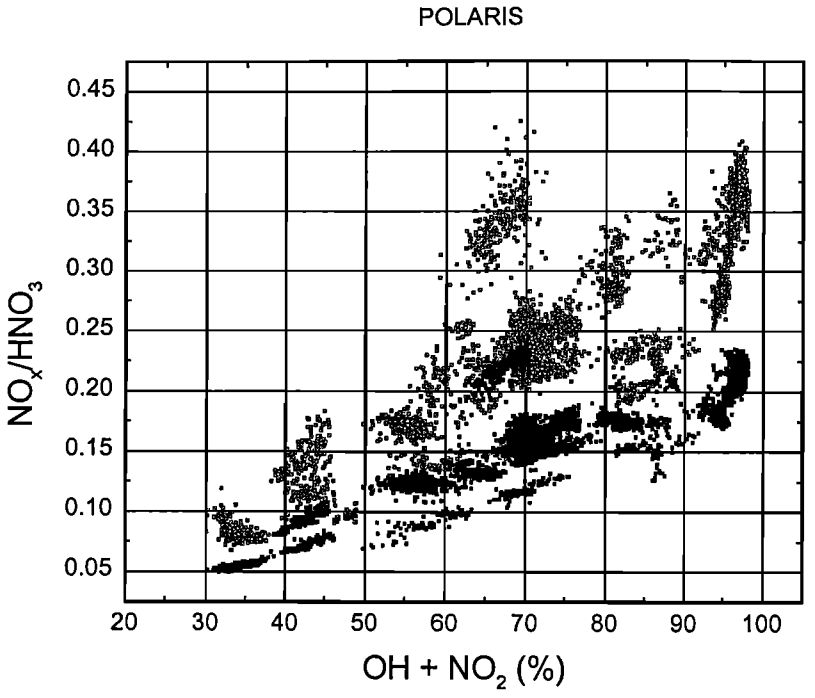

Figure 10. Observed (gray) and calculated using JPL 1997 parameters (black) NO_x/HNO_3 as a function of the chemical coordinate $OH+NO_2$.

such as shown in Figure 11 will have a slope of zero if the two agree. Deviation of the slope from zero is an indicator of an error in the model (or the measurements) that is correlated with the chemical coordinate. In this case, a deviation of the slope from zero indicates an error in the rate of $OH+NO_2$, N_2O_5 hydrolysis or both. Changes to the rate of $OH+HNO_3$ in the Rates '99 model have no effect on the slope because we hold the relative contribution of this rate constant in the comparison. A linear least squares fit to the observation-model comparison has a positive slope of 0.084%/(percent $OH+NO_2$) for the JPL '97 model and 0.012%/(percent $OH+NO_2$) for the rates '99 model, with a statistical uncertainty of 0.0065%/%. The slopes indicate the ratio of the rate of N_2O_5 hydrolysis to the rate of the $OH+NO_2$ reaction is 8.4% too small in the JPL 1997 model and 1.2% too small in the rates '99 model. If the statistical uncertainty were the dominant uncertainty and NO_x were always small compared to HNO_3 (so that increases in NO_x don't result in decreases in

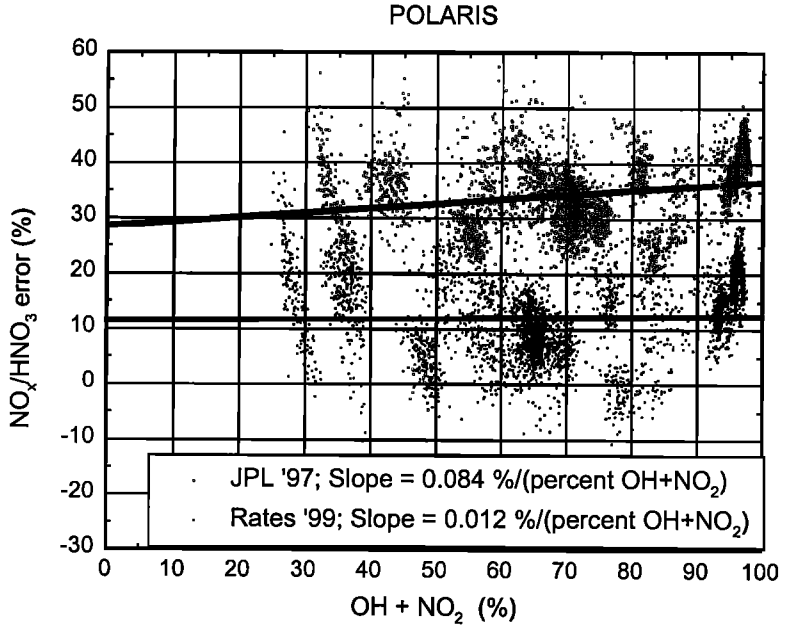

Figure 11. Percent error in the model representation of NO_x/HNO_3 as a function of the $OH+NO_2$ chemical coordinate. Fits to the data are shown indicating slopes of +0.084%/(percent $OH+NO_2$) for the JPL 1997 model (gray) and +0.012%/(percent $OH+NO_2$) for the rates '99 model (black).

HNO_3), then the slope in the JPL 1997 model could be reduced to zero by an 8% increase in the rate of N_2O_5 hydrolysis, an 8% decrease in the rate of the $OH+NO_2$ reaction, or a combination of changes in the two rates that is equivalent. The recommendations of *Dransfield et al.* [1999] and *Brown et al.* [1999a] reduce the rate of $OH+NO_2$ by 14% at 225 K and $[M]=2x10^{18}$ molecules/cm^3. The model requires more than an 8% change in the rate to achieve near perfect agreement because NO_x is over 1/3 of NO_y at 100% along the $OH+NO_2$ coordinate. A crude estimate suggests the 14% increase in NO_x resulting from slowing the NO_x loss rate, reduces the HNO_3 abundance by about 5% and the NO_x production rate by that same 5%. As a result, the net change in NO_x is approximately the difference between these two numbers or 9%. The 7% change in slope that occurs in a more detailed calculation using the full model and Rates '99 input is consistent with this estimate.

Since the slope error (8%) in the JPL 1997 model is small compared to the mean difference between the model and the observations of 33.5%, the chemical coordinate analysis demonstrates that no single fix would bring the JPL 1997 model and observations into perfect agreement. For example, again for simplicity neglecting the coupling to HNO_3, if the 35% decrease in the rate of $OH+NO_2$ (relative to JPL 1997) suggested by *Osterman et al.* [1999] were implemented, there would be nearly exact agreement between model and measurements at the point 100% along the $OH+NO_2$ coordinate. However, the change would have no effect at 0% along this coordinate. At 40% along the $OH+NO_2$ coordinate the change would be approximately 40%×35%=14%. As a result, the slope of the model-measurement comparison would change from +0.08%/(percent $OH+NO_2$) to approximately -0.27%/(percent OH + NO_2), increasing by threefold the magnitude and changing the sign of the error made evident through use of the chemical coordinates. The coupling of NO_x and HNO_3 abundances reduces the severe error predicted by this uncoupled model but not enough to produce a near zero slope.

Thus far, we deferred discussion of the systematic uncertainty in this analysis of NO_x/HNO_3 photochemistry. The observation of nearly perfect agreement, a slope of 0.01%/(percent $OH+NO_2$), between the observations and the rates '99 model is remarkable. An a priori estimate of the accuracy of the ratio of N_2O_5 hydrolysis to $OH+NO_2$ depends on three rate coefficients, (k_{OH+NO2}, $k_{N2O5+H2O}$, and k_{NO2+O3}), and measurements of [SA], [O_3], and [OH]. With the exception of O_3 (5%), each of these terms is uncertain to at least 20% leading to an estimate of at least 45% uncertainty (assuming the uncertainties add in quadrature). Perhaps the near perfect agreement is fortuitous, perhaps it results from a propensity for laboratory scientists to focus attention on weeding out of errors in rate constants and observations in response to discrepancies identified in prior comparisons of observations and models, or perhaps it results from overly conservative estimates of the uncertainty in the rate constants and the observations. Understanding the reasons for the better than expected agreement is important to accurately characterizing uncertainty in model predictions of the behavior of the atmosphere in the future and to weighing the import of differences between comparison of models and observations.

The significance of the slopes shown in Figure 11 depends directly on the precise calibration of the measurements. That is to say, despite overall uncertainty of 20% associated with possible systematic errors in the measurements (calibration gases, absorption cross sections, ...), the relative error of measurements obtained at different times or at different locations in the chemical phase space is dominated by random noise that can be reduced by averaging. The most severe limitations to our analysis thus arise from (1) flight-to-flight imprecision in the instrument calibration and (2) the effects of projection from the six primary coordinates to these two aggregate coordinates. Some of the variability shown in Figure11 results from these effects. Assessment of the uncertainty in the analysis depends on the assumption that, over the full range in the $OH+NO_2$ coordinate, we have randomly sampled the deviations associated with other coordinates and flight-to-flight imprecision. The presence of two populations of observations at $OH+NO_2$ ≈80% suggests we have at least sampled some range of deviations.

Given this uncertainty, we estimate the constraints placed on the model by the chemical coordinate comparison by assuming a ±15% uncertainty about the mean of the points at three positions along the $OH+NO_2$ coordinate, Figure 12. The choice of ±15% is somewhat arbitrary, but reflects an assessment that the distribution about the mean deviation of the model from the observations is likely represented within the range of the present sample. For the rates '99 model the mean of the observations at the two extreme points along the chemical coordinate is +20% and +15%. Note that these values do not lie along the best fit line of Figure 11 because the lines in Figure 11 are strongly weighted by the large number of observations at values of 60% or greater along the $OH+NO_2$ coordinate. Using the ±15% uncertainty constraint, shown as the error bars in Figure 12, we find the slope of the rates '99 model-measurement comparison is bounded by an uncertainty of +30%, -45%. It is purely coincidental that the lines constrained by the error bars have intercepts near zero. Analysis of observations at lower $OH+NO_2$ such as were obtained in the SPADE, ASHOE, and STRAT campaigns could reduce this uncertainty to ±30%. Reductions beyond that require an improved understanding of the factors that contribute to a spread in the agreement at a single value along the chemical coordinate.

The rates '99 model-measurement comparison along the NO_2 loss chemical coordinate is within experimental uncertainty. The slope error is barely statistically different from zero, and the mean value of the error is 11%, well within the ±20% absolute uncertainty in the observed ratio of NO_x/HNO_3. However, we note that the mean error is weighted by the large majority of observations at 65% along the $OH+NO_2$ chemical coordinate. At lower and higher positions along this coordinate, the error is larger. This indicates that additional changes to models of the photochemistry governing NO_x abundances are necessary to accurately describe the atmosphere. The data do not exclude the possibility of rate constant revisions as large as those implemented in Rates '99. Analysis of prior observations that extend the experimental data base to lower values along the $OH+NO_2$ coordinate and new observations that increase the range of the data along other chemical coordinates will make it possible to isolate individual factors affecting the NO_x loss processes.

However, further improvement in the model-measurement comparison beyond that of rates '99 is likely to involve processes or measurements that do not have a differential effect on the rates of $OH+NO_2$ and N_2O_5 hydrolysis. If

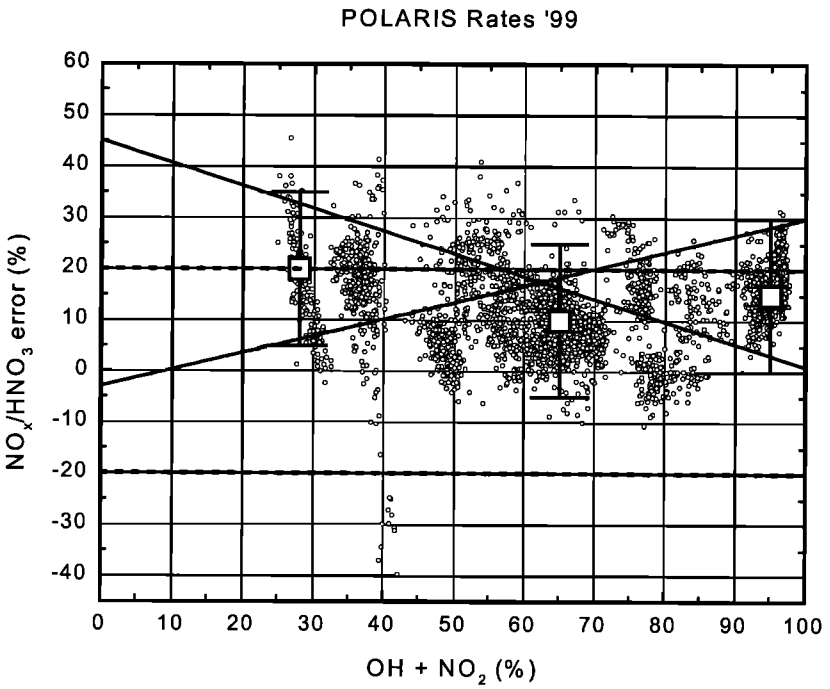

Figure 12. Percent error in the rates '99 representation of NO_x/HNO_3 as a function of the $OH+NO_2$ chemical coordinate. The large points represent the average value at that position along the chemical coordinate, and the error bars represent an estimate of the possible systematic errors resulting from finite sampling and compressing other variables onto this single coordinate. The dashed lines are the experimental error limits. The black lines represent the range of constraints on the ratio of the rate of $OH+NO_2$ to the sequence of processes leading to N_2O_5 hydrolysis.

changes to the kinetics of reactions affecting either of these processes are identified (either from analysis of atmospheric observations or from laboratory experiments) in the future, the analysis presented here indicates that a model attempting to represent atmospheric observations should make changes to both reaction sets in tandem.

4.4. Model Evaluation-NO_x Sources

In contrast to the information the POLARIS data offers about NO_2 sinks, it offers little information about the rate of NO_2 sources. Figure 13 shows the percentage error of NO_x/NO_y as a function of the fraction of NO_x produced by HNO_3 photolysis. The figure includes a large error bar reflecting the systematic uncertainties associated with the observations alone. The horizontal lines at the top and bottom of this error bar are drawn across the full range in the HNO_3 photolysis coordinate for which we have observations. Any line that passes through the observations without crossing these lines will be consistent with the measurements, leaving open the possibility of large negative errors at $HNO_3+h\nu$ =0% coupled to large positive errors at $HNO_3+h\nu$ =100%. In this sense, the measurements do place some limits on the relative rate coefficients. For example, it would be inconsistent with the observations to suggest that both the photolysis and the OH reactions of HNO_3 are 50% faster than in the rates '99 model. In an attempt to be more quantitative, we show two lines in Figure 13, originating at an assumed 0% error in the HNO_3 photolysis rate coefficient and passing through the upper limits set by the systematic errors in the observations. The lines pass within the ±20% uncertainty associated with possible systematic errors in the observations terminating at –13% and +53%. These numbers are lower bounds on the uncertainty in the $OH+HNO_3$ reaction rate derived from observations since they are based on the premise that every other element of the model and observations is perfectly accurate. The range of 66% uncertainty is comparable to the range estimated for the product of the rate coefficient $k_{OH+HNO3}$ and [OH].

The small range in the NO_x production coordinate results from strong correlations between 24 hour integrated [OH] and 24-hour integrated HNO_3 photolysis. At higher and lower altitudes, different relationships between these two can be observed, expanding the range of phase-space that can be accessed in the atmosphere. *Jucks et al.* [1999] present analysis of observations in the chemical coordinates developed here that range from 30-100% in the $OH+NO_2$ coordinate and 40-90% in the HNO_3 photolysis coordinate. Using the chemical coordinate approach, they show evidence of a substantial error (~70%) in the relative rates of $OH+HNO_3$ and $HNO_3+h\nu$ using a model based on JPL 1997 kinetics and as much as a 40% error in the relative rates of these processes using a model with inputs similar to our rates '99.

5. Conclusions

Recent progress in reproducing observed ozone trends in 2-D models [*Jackman et al.*, 1996; *Solomon et al.*, 1998] has brought renewed attention to whether such agreement is numerically significant given the uncertainties in the input parameters to these models. The inability of the transport formulation of most models to reproduce the observed age

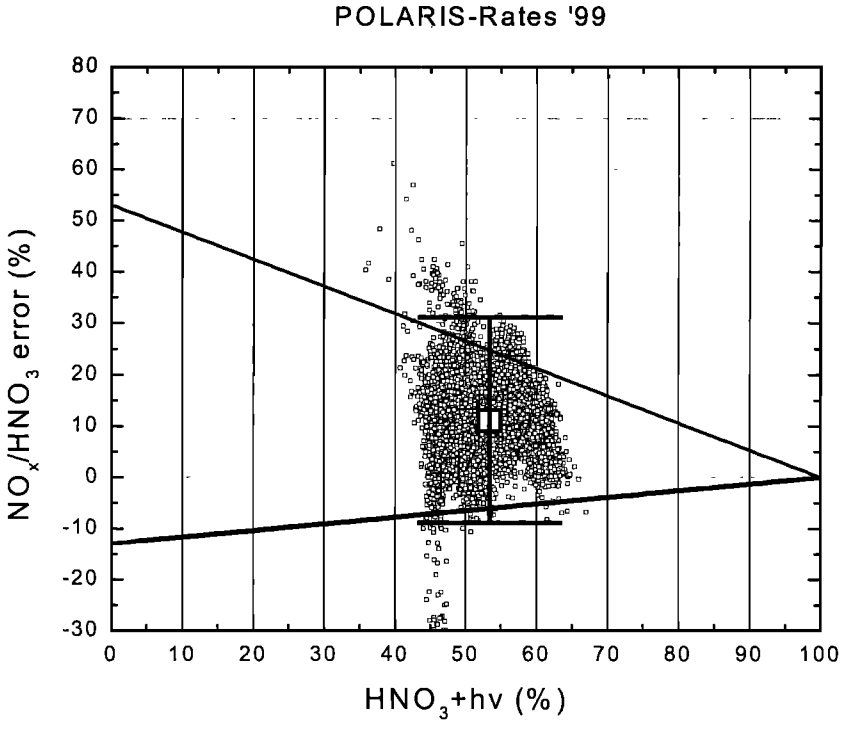

Figure 13. Percent error in the rates '99 representation of NO_x/HNO_3 as a function of the NO_2 production that occurs via photolysis of HNO_3. The mean error is +11%. The large error bar reflects our estimate of the systematic error associated with mean of these points, and the horizontal extent of this bar is significant, reflecting the range in the HNO_3 +$h\nu$ over which we constrain the model with observations. The two lines are used to estimate of the maximum error (-13%, +53%) in the OH+HNO_3 rate that would be consistent with the observations and the assumption that the model and measurements are perfectly accurate at the 100% HNO_3 photolysis rate limit.

distribution of stratospheric air [*Boering et al.*, 1996; *Andrews et al.*, 1999; *Fleming et al.*, 1999; *Hall et al.*, 1999] raises further questions about how the chemical component of the models can appear "correct" in the presence of substantial transport errors. *Considine et al.* [1999] address part of this problem by performing Monte Carlo analysis of the sensitivity of ozone trends to uncertainty in rate coefficients for gas phase bimolecular, photolytic, and heterogeneous reactions. They showed that differences between model calculations of trends and observations are not significant, if the estimates of uncertainty in reaction coefficients provided by JPL 1997 are representative of the true uncertainty. As part of an effort to quantitatively evaluate how well we understand stratospheric photochemistry, in this paper, we present a chemical coordinate analysis that provides an assessment of the accuracy and uncertainty of some of the key aspects of $NO_x \Leftrightarrow NO_y$ photochemistry.

1. On average, the POLARIS observations confirm that models of the NO_x partitioning between NO to NO_2 ratio are accurate. Assuming current models are complete, the measurements are consistent with the models to within 2.6%. However, the results also suggest there is a temperature-dependent error and an albedo related error in calculations of the ratio J_{NO2}/k_{NO+O3}. Since J_{NO2} and the minor contributions to NO_x partitioning have a very weak temperature dependence, our analysis indicates the temperature dependence of the rate coefficient for $NO+O_3$ is too steep. A rate expression of $Ae^{-Ea/(RT)}$ with $A= 9x10^{-13}$ and E_a=10 kJ/mol improves the description of the temperature dependence in the range 215-235 K as does the more complex expression recommended by *Borders and Birks* [1982]. Models using the JPL 1997 recommendations for uncertainty, as a priori uncertainty estimates, will substantially overestimate the uncertainty in NO_x partitioning. We recommend an uncertainty of ±16% in the quantity J_{NO2}/k_{NO+O3} independent of temperature ($215<T<235$). For the temperature-dependent uncertainty in the $NO+O_3$ rate coefficient, we recommend using the Borders and Birks expression without a temperature-dependent uncertainty, or using an Arrhenius expression with the constants indicated above and an uncertainty in E_a/R of ±150. For the JPL 1997 constants an uncertainty in E_a/R of +0/-300 would better overlap the observations than the current ±200. After completion of this analysis, the JPL 2000 recommendation was published with an increase of E_a/R of 100K relative to JPL 1997 [*Sander et al.*, 2000]. This new recommendation exacerbates the disagreement between models and observations at stratospheric temperatures.

2. Models employing the lower activation energy for $NO+O_3$ that we recommend will have higher NO_2/NO ratios at low temperature. Such models will have lower NO_x abundances because all NO_x loss processes pass through NO_2 with NO essentially an inert reservoir. The models will also have higher rates of HO_x catalysis due to the NO_x reduction and the reduced abundances of NO. The two effects on chlorine catalysis are of opposite sign. Reduced NO_x increases ClO abundances, while increases in NO_2 suppress ClO.

3. On average, the POLARIS observations show that using the JPL 1997 rate constants in a model leads to an

underestimate of the lower stratospheric NO_x to HNO_3 ratio. In the mean, a JPL 1997 model underestimates the NO_x to HNO_3 ratio by 33.5%. This is outside the range of experimental uncertainty. The rates '99 model underestimates NO_x/HNO_3 by on average 10%, within the bounds of experimental uncertainty. These numbers would be little affected by a different form of the $NO+O_3$ rate constant because the bulk of the data was obtained at a 230 K where the NO_x partitioning is accurately described by the JPL 1997 model.

4. The POLARIS observations show that the relative rates of $OH+NO_2$ and the sequence of reactions leading to N_2O_5 hydrolysis are better represented by models that use an $OH+NO_2$ rate coefficient similar to the one suggested by *Dransfield et al.* [1999] or *Brown et al.* [1999a] than the one recommended by JPL 1997 [*DeMore et al.*, 1997]. The maximum relative error of the $OH+NO_2$ reaction rate to the N_2O_5 hydrolysis rate that is compatible with these observations is +30%/-45%. This more than halves the recommended uncertainty in the relative rates of these reactions, since the JPL 1997 recommendation for uncertainty in $N_2O_5 + H_2O$ alone is $\times\div 2$.

5. The POLARIS observations do not constrain the relative rates of $OH+HNO_3$ and $HNO_3+h\nu$ any better than the JPL 1997 recommendation. Both the JPL 1997 and the *Brown, et al.* [1999b] recommendations for the $OH+HNO_3$ rate coefficient are within the uncertainty defined by the chemical coordinate analysis.

Acknowledgments. The POLARIS experiments were supported by the NASA Upper Atmospheric Research Program and Atmospheric Effects of Aviation Project (M. Kurylo, P. DeCola, and R. Kawa, project managers). The $ClO/ClONO_2/NO_2$ instrument was developed with the support of the NASA Upper Atmospheric Research Program and the NASA Environmental Research Aircraft and Sensor Technology programs. Analyses presented in this paper were supported by NASA AEAP. K.K.P gratefully acknowledges an NSF graduate fellowship. We gratefully acknowledge the use of O_3 measurements obtained by J. J. Margitan and M. H. Proffitt, Chuck Brock's contribution to the aerosol measurements and both experimental contributions to NO, NO_2, and NO_y measurements, and comments on this paper by David Fahey and Ru-Shan Gao.

References

Andrews, A.E., K.A. Boering, B.C. Daube, S.C. Wofsy, E.J. Hintsa, E.M. Weinstock, and T.P. Bui, Empirical age spectra for the lower tropical stratosphere from in situ observations of CO_2: Implications for stratospheric transport, *J. Geophys. Res.*, *104*(D21), 26,581-26,595, 1999.

Birks, J.W., B. Shoemaker, T.J. Leck, and D.M. Hinton, Studies of reactions of importance in the stratosphere, I: Reaction of nitric oxide with ozone, *J. Chem. Phys.*, *65*(12), 5181-5185, 1976.

Boering, K.A., S.C. Wofsy, B.C. Daube, H.R. Schneider, M. Loewenstein, J.R. Podolske, and I.J. Conway, Stratospheric mean ages and transport rates from observations of carbon dioxide and nitrous oxide, *Science*, *274*(5291), 1340-1343, 1996.

Bonne, G.P., In situ measurements of chlorine nitrate in the lower stratosphere, Ph.D. thesis, Harvard Univ., Cambridge, Mass., 1998.

Bonne, G.P., et al., An examination of the inorganic chlorine budget in the lower stratosphere, *J. Geophys. Res.*, *105(D2)*, 1957-1971, 2000.

Borders, R.A., and J.W. Birks, High precision measurements of activation energies over small temperature intervals: Curvature in the Arrhenius plot for the reaction $NO+O_3 \rightarrow NO_2 + O_2$, *J. Phys. Chem.*, *86(17)*, 3295-3302, 1982.

Brown, S.S., R.K. Talukdar, and A.R. Ravishankara, Rate constants for the reaction $OH+NO_2+M$ to HNO_3+M under atmospheric conditions, *Chem. Phys. Lett.*, *299*(3-4), 277-284, 1999a.

Brown, S.S., R.K. Talukdar, and A.R. Ravishankara, Reconsideration of the rate constant for the reaction of hydroxyl radicals with nitric acid, *J. Phys. Chem. A*, *103*(16), 3031-3037, 1999b.

Brune, W.H., E.M. Weinstock, and J.G. Anderson, Midlatitude ClO below 22 km altitude: measurements with a new aircraft-borne instrument, *Geophys. Res. Lett.*, *15*(2), 144-147, 1988.

Cadle, R.D., P. Crutzen, and D. Ehhalt, Heterogeneous chemical reactions in the stratosphere, *J. Geophys. Res.*, *80*(24), 3381-5, 1975.

Cohen, R.C., et al., Are models of catalytic removal of O_3 by HO_x accurate? Constraints from in situ measurements of the OH to HO_2 ratio, *Geophys. Res. Lett.*, *21*(23), 2539-2542, 1994.

Considine, D.B., R.S. Stolarski, S.M. Hollandsworth, C.H. Jackman, and E.L. Fleming, A Monte Carlo uncertainty analysis of ozone trend predictions in a two-dimensional model, *J. Geophys. Res.*, *104*(D1), 1749-1765, 1999.

Crutzen, P.J., Ozone production rates in an oxygen-hydrogen-nitrogen oxide atmosphere, *J. Geophys Res.*, *76*(D30), 7311-7327, 1971.

Del Negro, L.A., et al., Comparison of modeled and observed values of NO_2 and J_{NO2} during the POLARIS mission, *J. Geophys. Res.*, *104*(D21), 26,687-26,704, 1999.

DeMore, W.B., S.P. Sander, C.J. Howard, A.R. Ravishankara, D.M. Golden, C.E. Kolb, R.F. Hampson, M.J. Kurylo, and M. Molina, Chemical kinetics and photochemical data for use in stratospheric modeling: evaluation number 12, JPL Publication 97-4, NASA Jet Propulsion Laboratory, Pasadena, Calif., 1997.

Dessler, A.E., S.R. Kawa, A.R. Douglass, D.B. Considine, J.B. Kumer, A.E. Roche, J.L. Mergenthaler, J.W. Waters, J.M. Russell, III, and J.C. Gille, A test of the partitioning between ClO and $ClONO_2$ using simultaneous UARS measurements of ClO, NO_2, and $ClONO_2$, *J. Geophys. Res.*, *101*(D7), 12,515-12,521, 1996.

Donahue, N.M., M.K. Dubey, R. Mohrschladt, K.L. Demerjian, and J.G. Anderson, High-pressure flow study of the reactions $OH+NO_x$ to $HONO_x$: Errors in the falloff region, *J. Geophys. Res.*, *102*(D5), 6159-6168, 1997.

Dransfield, T.J., K.K. Perkins, N.M. Donahue, J.G. Anderson, M.M. Sprengnether, and K.L. Demerjian, Temperature- and pressure-dependent kinetics of the gas-phase reaction of the hydroxyl radical with nitrogen dioxide, *Geophys. Res. Lett.*, *26*(6), 687-690, 1999.

Drdla, K., R.F. Pueschel, A.W. Strawa, R.C. Cohen, T.F. Hanisco, and R.J. Salawitch, Microphysics and chemistry of sulfate aerosols at warm stratospheric temperatures, *J. Geophys. Res.*, *104*(D21), 26,737-26,751, 1999.

Fahey, D.W., D.M. Murphy, K.K. Kelly, M.K.W. Ko, M.H. Proffitt, C.S. Eubank, G.V. Ferry, M. Loewenstein, and K.R. Chan, Measurements of nitric oxide and total reactive nitrogen in the Antarctic stratosphere: observations and chemical implications, *J. Geophys, Res.*, *94*(D14), 16,665-16,681, 1989.

Fahey, D.W., et al., In situ measurements constraining the role of sulphate aerosols in mid-latitude ozone depletion, *Nature*, *363*(6429), 509-514, 1993.

Fleming, E.L., C.H. Jackman, R.S. Stolarski, and D.B. Considine, Simulation of stratospheric tracers using an improved empirically based two-dimensional model transport formulation, *J. Geophys. Res.*, *104*(D19), 23,911-23,934, 1999.

Fong, C., and W.H. Brune, A laser induced fluorescence instrument for measuring tropospheric NO_2, *Rev. Sci. Inst.*, *68*(11), 4253-4262, 1997.

Gao, R.S., et al., Partitioning of the reactive nitrogen reservoir in the lower stratosphere of the southern hemisphere: Observations and modeling, *J. Geophys. Res.*, *102*(D3), 3935-3949, 1997.

Gao, R.S., et al., A Comparison of Observations and Model Simulations of NO_x/NO_y in the Lower Stratosphere, *Geophys. Res. Lett.*, *26*(8), 1153-1156, 1999.

George, L.A., and R.J. O'Brien, Prototype FAGE Determination of NO_2, *J. Atmos. Chem.*, *12*, 195-209, 1991.

Gordley, L.L., et al., Validation of nitric oxide and nitrogen dioxide measurements made by the Halogen Occultation Experiment for UARS platform, *J. Geophys. Res.*, *10* (D6), 10,241-10,266, 1996.

Hall, T.M., D.W. Waugh, K.A. Boering, and R.A. Plumb, Evaluation of transport in stratospheric models, *J. Geophys. Res.*, *104*(D15), 18,815-18,839, 1999.

Harries, J.E., Stratospheric composition measurements as a test of photochemical theory, *J. Atmos. Terr. Phys.*, *44*(7), 591-597, 1982.

Hintsa, E.J., E.M. Weinstock, J.G. Anderson, R.D. May, and D.F. Hurst, On the accuracy of in situ water vapor measurements in the troposphere and 'ower stratosphere with the Harvard Lyman-alpha hygrometer, *J. Geophys. Res.*, *104*(D7), 8183-8189, 1999.

Jackman, C.H., E.L. Fleming, S. Chandra, D.B. Considine, and J.E. Rosenfield, Past, present, and future modeled ozone trends with comparisons to observed trends, *J. Geophys. Res.*, *101*(D22), 28,753-28,767, 1996.

Jaegle, L., et al., In situ measurements of the NO_2/NO ratio for testing atmospheric photochemical models, *Geophys. Res. Lett.*, *21*(23), 2555-2558, 1994.

Johnston, H.S., Reduction of Stratospheric Ozone by Nitrogen Oxide Catalysts from Supersonic transport Exhaust, *Science*, *173(3996)*, 517-522, 1971.

Jonsson, H.H., et al., Performance of a focused cavity aerosol spectrometer for measurements in the stratosphere of particle size in the 0.06-2.0- /symbol mu/m-diameter range, *J. Atmos Oceanic Technol.*, *12*(1), 115-129, 1995.

Jucks, J.W., D.G. Johnson, K.V. Chance, W.A. Traub, and R.J. Salawitch, Nitric acid in the middle stratosphere as a function of altitude and aerosol loading, *J. Geophys. Res* , *104*(D21), 26,715-26,724, 1999.

Koike, M., N.B. Jones, W.A. Matthews, P.V. Johnston, R.L. McKenzie, D. Kinnison, and J. Rodriguez, Impact of Pinatubo aerosols on the partitioning between NO_2 and HNO_3, *Geophys. Res. Lett.*, *21*(7), 597-600, 1994.

Kumer, J.B., S.R. Kawa, A.E. Roche, J.L. Mergenthaler, S.E. Smith, F.W. Taylor, P.S. Connell, and A.R. Douglass, UARS first global N_2O_5 data sets: application to a stratospheric warming event in January 1992, *J. Geophys. Res.*, *102*(D3), 3575-3582, 1997.

McElroy, C.T., A spectroradiometer for the measurement of direct and scattered solar irradiance from on board the NASA ER-2 high-altitude research aircraft, *Geophys. Res. Lett.*, *22*(11), 1361-1364, 1995.

McElroy, M.B., R.J. Salawitch, and K. Minschwaner, The changing stratosphere, *Planet. Space Sci.*, *40*(2-3), 373-401, 1992.

Michael, J.V., J.E. Allen Jr., and W.D. Brobst, Temperature dependence of the NO+O_3 reaction rate from 195 to 369K, *J. Phys. Chem.*, *85(26)*, 4109-4117, 1981.

Mickley, L.J., J.P.D. Abbatt, J.E. Frederick, and J.M. Russell III, Response of summertime odd nitrogen and ozone at 17 mbar to Mount Pinatubo aerosol over the southern midlatitudes: observations from the Halogen Occultation Experiment, *J. Geophys. Res.*, *102*(D19), 23,573-23,582, 1997.

Moonen, P.C., J.N. Cape, R.L. StoretonWest, and R. McColm, Measurement of the NO - O_3 reaction rate at atmospheric pressure using realistic mixing ratios, *J Atmos. Chem.*, *29*, 299-314, 1998.

Mozurkewich, M., and J.G. Calvert, Reaction probability of N_2O_5 on aqueous aerosols, *J. Geophys. Res.*, *93*(D12), 15,889-15,896, 1988.

Newchurch, M.J., et al., Stratospheric NO and NO_2 abundances from ATMOS solar-occultation measurements, *Geophys. Res. Lett.*, *23*(17), 2373-2376, 1996.

Nickolaisen, S.L., S.P. Sander, and R.R. Friedl, Pressure-Dependent Yields and Product Branching Ratios in the Broadband Photolysis of Chlorine Nitrate, *J. Phys. Chem.*, *100*(24), 10,165-10,178, 1996.

Noxon, J.F., Nitrogen dioxide in the stratosphere and troposphere measured by ground-based absorption spectroscopy, *Science*, *189*(4202), 547-549, 1975.

Osterman, G.B., B. Sen, G.C. Toon, R.J. Salawitch, J.J. Margitan, J.-F. Blavier, D.W. Fahey, and R.S. Gao, Partitioning of NO_y species in the summer Arctic stratosphere, *Geophys. Res. Lett.*, *26*(8), 1157-1160, 1999.

Perkins, K.K., In situ observations of nitrogen dioxide using laser-induced fluorescence detection: Examining the NO_x-HNO_3 system in the lower stratosphere, Ph.D. thesis, Harvard Univ., Cambridge, Mass., 2000.

Podolske, J., and M. Loewenstein, Airborne tunable diode laser spectrometer for trace-gas measurement in the lower stratosphere, *Appl. Opt.*, *32*(27), 5324-5333, 1993.

Prather, M.J., Ozone in the upper stratosphere and mesosphere, *J. Geophys. Res.*, *86*(C6), 5325-5338, 1981.

Proffitt, M.H., and R.J. McLaughlin, Fast-response dual-beam UV-absorption ozone photometer suitable for use on stratospheric balloons, *Rev. Sci. Inst.*, *54*(12), 1719-28, 1983.

Ray, G.W., and R.T. Watson, Kinetics of the reaction NO + O_3 -> NO_2 + O_2 from 212 to 422K, *J. Phys. Chem.*, *85(12)*, 1673-1676, 1981.

Roche, A.E., J.B. Kumer, J.L. Mergenthaler, R.W. Nightingale, W.G. Uplinger, G.A. Ely, J.F. Potter, D.J. Wuebbles, P.S. Connell, and D.E. Kinnison, Observations of lower-stratospheric $ClONO_2$, HNO_3, and aerosol by the UARS CLAES experiment between January 1992 and April 1993, *Journal of the Atmospheric Sciences*, *51*(20), 2877-902, 1994.

Salawitch, R.J., et al., The diurnal variation of hydrogen, nitrogen, and chlorine radicals: implications for the heterogeneous production of HNO_2, *Geophys. Res Lett.*, *21*(23), 2551-2554, 1994.

Sander, S.P., et al., Chemical kinetics and photochemical data for use in stratospheric modeling supplement to evaluation 12: Update of key reactions evaluation number 13, JPL Publication 00-003, NASA-Jet Propulsion Laboratory, Pasadena, Calif., 2000.

Scott, S.G., T. P. Bui, K. R. Chan, and S.W. Bowen, The Meteorological Measurement System on the NASA ER-2 aircraft, *J. Atmos. Oceanic Technol.*, *7*(4), 525-40, 1990.

Sen, B., G.C. Toon, G.B. Osterman, J.F. Blavier, J.J. Margitan, R.J. Salawitch, and G.K. Yue, Measurements of reactive nitrogen in the stratosphere, *J. Geophys. Res.*, *103*(D3), 3571-3585, 1998.

Slusser, J., X. Liu, K. Stamnes, G. Shaw, R. Smith, R. Storvold, F. Murcray, A. Lee, and P. Good, High-latitude stratospheric NO_2 and HNO_3 over Fairbanks (65°N) 1992-1994, *J. Geophys. Res.*, *103*(D1), 1549-1554, 1998.

Solomon, S., R.W. Sanders, R.O. Jakoubek, K.H. Arpag, S.L. Stephens, J.G. Keys, and R.R. Garcia, Visible and near-ultraviolet spectroscopy at McMurdo Station, Antarctica, 10, Reductions of stratospheric NO_2 due to Pinatubo aerosols, *J. Geophys. Res.*, *99*(D2), 3509-3516, 1994.

Solomon, S., R W. Portmann, R.R. Garcia, W. Randel, F. Wu, R. Nagatani, J. Gleason, L. Thomason, L.R. Poole, and M.P. McCormick, Ozone depletion at midlatitudes: Coupling of volcanic aerosols and temperature variability to anthropogenic chlorine, *Geophys Res. Lett* , *25*(11), 1871-1874, 1998.

Stimpfle, R.M., et al., The coupling of $ClONO_2$, ClO and NO_2 from in situ observations using the NASA ER-2 aircraft, *J Geophys Res.*, *104*(D21), 26,705-26,714, 1999.

Stimpfle, R M., et al., The response of ClO radical concentrations to variations in NO_2 radical concentrations in the lower stratosphere, *Geophys. Res. Lett.*, *21*(23), 2543-2546, 1994

Stolarski, R.S., et al., 1995 scientific assessment of the atmospheric effects of stratospheric aircraft, NASA Reference Publication 1381, 1995.

Thornton, J.A., P J. Wooldridge, and R.C. Cohen, Atmospheric NO_2: In situ laser-induced fluorescence detection at parts per trillion mixing ratios, *Anal Chem* , *72*(3), 528-539, 2000.

Wamsley, P.R., et al., Distribution of halon-1211 in the upper troposphere and lower stratosphere and the 1994 total bromine budget, *J. Geophys Res* , *103*(D1), 1513-1526, 1998.

Webster, C.R., R.D. May, R. Toumi, and J.A. Pyle, Active nitrogen partitioning and the nighttime formation of N_2O_5 in the stratosphere· Simultaneous in situ measurements of NO, NO_2, HNO_3, O_3, and N_2O using the BLISS diode laser spectrometer, *J. Geophys Res.*, 95(D9) 13,851-13,866, 1990.

Webster, C.R., R.D. May, M. Allen, L. Jaegle, and M.P. McCormick, Balloon profiles of stratospheric NO_2 and HNO_3 for testing the heterogeneous hydrolysis of N_2O_5 on sulfate aerosols, *Geophys. Res. Lett.*, *21*(1), 53-56, 1994a.

Webster, C.R., R.D. May, C.A. Trimble, R.G. Chave, and J. Kendall, Aircraft (ER-2) Laser Infrared Absorption Spectrometer (ALIAS) For In Situ Stratospheric Measurements of HCl, N_2O, CH_4, NO_2, and HNO_3, *Appl. Opt.*, *33*, 454-472, 1994b.

Weinheimer, A.J., J.G. Walega, B.A. Ridley, B.L. Gary, D.R. Blake, N.J. Blake, F.S. Rowland, G.W. Sachse, B.E. Anderson, and J.E. Collins, Meridional distributions of NO_x, NO_y, and other species in the lower stratosphere and upper troposphere during AASE II, *Geophys. Res. Lett.*, *21*(23), 2583-2586, 1994.

Wennberg, P.O., R.C. Cohen, N.L. Hazen, L.B. Lapson, N.T. Allen, T.F. Hanisco, J.F. Oliver, N.W. Lanham, J.N. Demusz, and J.G. Anderson, Aircraft-borne, laser-induced fluorescence instrument for the in situ detection of hydroxyl and hydroperoxyl radicals, *Rev. of Sci Inst.*, *65*(6), 1858-1876, 1994a.

Wennberg, P.O., et al., Removal of stratospheric O_3 by radicals: In

situ measurements of OH, HO_2, NO, NO_2, ClO, and BrO, *Science*, *266*(5184), 398-404, 1994b.

Wennberg, P.O., et al., Twilight observations suggest unknown sources of HO_x, *Geophys. Res. Lett.*, *26*(10), 1373-1376, 1999.

Zhou, D.K., G.E. Bingham, B.K. Rezai, G.P. Anderson, D.R. Smith, and R.M. Nadile, Stratospheric CH_4, N_2O, H_2O, NO_2, N_2O_5, and $ClONO_2$ profiles retrieved from Cryogenic Infrared Radiance Instrumentation for Shuttle (CIRRIS 1A)/STS 39 measurements, *J. Geophys. Res.*, *102*(D3), 3559-3573, 1997.

G. P. Bonne, Electric Power Research Institute, Palo Alto, California, 94304.

T. P. Bui, Ames Research Center, NASA, Moffett Field, California, 94035-1000.

R. C. Cohen, Department of Chemistry, University of California, Berkeley, 94720-1460 (cohen@cchem.berkeley.edu).

L. A. Del Negro, Climate Monitoring and Diagnostics Laboratory, NOAA, Boulder, Colorado, 80303.

T. F. Hanisco, E. J. Lanzendorf, R. M. Stimpfle, P. B. Voss, Department of Chemistry and Chemical Biology, Harvard University, Cambridge, Massachusetts, 02138.

L. C. Koch, Department of Chemistry, University of Colorado, Boulder, 80309.

C. T. McElroy, Environment Canada, Downsview, Ontario, Canada, M3H 5T4.

K. K. Perkins, Department of Earth and Planetary Sciences, Harvard University, Cambridge, Massachusetts, 02138.

R. J. Salawitch, Jet Propulsion Laboratory, California Institute of Technology, Pasadena, 91125.

P. O. Wennberg, Divisions of Geological and Planetary Sciences, California Institute of Technology, Pasadena, 91125.

J. C. Wilson, Department of Mechanical Engineering, University of Denver, Denver, Colorado, 80208.

(Received February 23, 2000; revised May 1, 2000;
accepted May 8, 2000.)